Holocene record of Tuggerah Lake estuary development on the Australian east coast: Sedimentary responses to sea-level fluctuations and climate variability

Peter I. Macreadie [a,b,]*, Timothy C. Rolph [c], Claudia Schröder-Adams [d], Ron Boyd [e], Charles G. Skilbeck [f]

[a] Plant Functional Biology and Climate Change Cluster, University of Technology Sydney, Broadway, New South Wales 2007, Australia
[b] Centre for Integrative Ecology, School of Life and Environmental Sciences, Faculty of Science, Engineering and Built Environment, Deakin University, Burwood, Victoria 3125, Australia
[c] BP America Inc., 200 Westlake Park Boulevard, Houston, TX, USA
[d] Department of Earth Sciences, Carleton University, Ontario K1S 5B6, Canada
[e] School of Geosciences, University of Newcastle, Callaghan 2308, Australia
[f] School of the Environment, University of Technology Sydney, Broadway, New South Wales 2007, Australia

ABSTRACT

We investigated the Holocene palaeo-environmental record of the Tuggerah Lake barrier estuary on the south-east coast of Australia to determine the influence of local, regional and global environmental changes on estuary development. Using multi-proxy approaches, we identified significant down-core variation in sediment cores relating to sea-level rise and regional climate change. Following erosion of the antecedent land surface during the post-glacial marine transgression, sediment began to accumulate at the more seaward location at ∼8500 years before present, some 1500 years prior to barrier emplacement and ∼4000 years earlier than at the landward site. The delay in sediment accumulation at the landward site was a consequence of exposure to wave action prior to barrier emplacement, and due to high river flows of the mid-Holocene post-barrier emplacement. As a consequence of the mid-Holocene reduction in river flows, coupled with a moderate decline in sea-level, the lake experienced major changes in conditions at ∼4000 years before present. The entrance channel connecting the lake with the ocean became periodically constricted, producing cyclic alternation between intervals of fluvial- and marine-dominated conditions. Overall, this study provides a detailed, multi-proxy investigation of the physical evolution of Tuggerah Lake with causative environmental processes that have influenced development of the estuary.

© 2015 The Authors. Published by Elsevier Ltd. This is an open access article under the CC BY-NC-ND license (http://creativecommons.org/licenses/by-nc-nd/4.0/).

1. Introduction

Barrier estuaries on the New South Wales (NSW; Australia) coastline developed following the sea level rise that accompanied the transition to the present interglacial climate [54]. In Tuggerah Lake, a barrier estuary on the mid-NSW coast, sediments began to accumulate at ∼9000 cal. years BP, behind relict Pleistocene barriers inundated during the post-glacial marine transgression [54]. Continued sea level rise, accompanied by the reworking of shelf sand bodies, supplied abundant marine sand to the estuaries during the early Holocene [61]; tidal sand bodies developed within the incised portion of the relict barrier, while a composite barrier system developed from the accumulation of contemporary sand on top of a relict, Pleistocene core (e.g. Lake Macquarie; [52]).

The supply of marine sand decreased abruptly at ∼6000 radiocarbon BP (∼6800 cal. years BP) shortly after the sea level highstand was reached [61,55]. Subsequently, the barrier heights have been increased by the development of storm ridges and dunes, while rivers have been the dominant supply of clastic material to the estuaries. Estimates of the timing and elevation of sea level at highstand vary; while the model of Thom and Roy [62] has highstand occurring between 6800 and 6400 radiocarbon years BP (7600–7200 cal. years BP), with a sea level within ±1 m of present mean sea level (msl), results from other studies (e.g. [2]) suggest that high-stand, at perhaps 2 m above present msl was achieved as early as 7000 radiocarbon years BP (7800 cal. years BP) and that sea-level has exceeded the present value for much of the mid- to late-Holocene.

* Corresponding author at: Plant Functional Biology and Climate Change Cluster, University of Technology Sydney, Broadway, New South Wales 2007, Australia.
E-mail address: peter.macreadie@uts.edu.au (P.I. Macreadie).

The goal of this study was to provide the first detailed, multi-proxy palaeo-reconstruction of the Holocene history of Tuggerah Lake. Through analysis of a suite of geochemical, sedimentological, and magnetic proxies, we have been able to provide new insight into how the estuary developed, and, importantly, the causative environmental processes (e.g. sea-level fluctuations) and regional development (urbanisation) that have influenced the development of the Lake.

2. Methods

Study site.

2.1. Modern environment and geology

Tuggerah Lake is a shallow (max depth <4 m) brackish to saline barrier estuary; the largest of the Tuggerah–Munmorah–Budgewoi lake system (Fig. 1). The lake lies behind a Holocene and Pleistocene coastal sand barrier complex that stretches between headlands located at the northern and southern margins. Tidal exchange currently occurs through a shallow, ephemeral inlet, "The Entrance", located at the southern limit of the Holocene barrier. Tidal exchange is restricted to ~1% of total lake volume and shoaling has closed the inlet completely on nine occasions in the last 100 years. The inlet restriction currently prevents the influx of marine sand to the lake; however, wave action is responsible for the southerly-directed transport of reworked sand from the flood-tide delta.

Freshwater enters the lake mainly from Ourimbah Creek and the Wyong River; fluvial sediment is currently accumulating in bay-head deltas and within the central estuarine basin [20]. The average annual rainfall of ~1200 mm (30-year average; Commonwealth of Australia, Bureau of Meteorology) is biased towards the months January–April and is strongly modulated by ENSO-band variability [59]. In eastern Australia, lower than average rainfall is associated with the negative phase (El Niño) of the Southern Oscillation Index (SOI), while higher rainfall accompanies the positive phase (La Niña) [48]. Rainfall (and stream-flow) is further enhanced when a La Niña event is concurrent with the negative phase of the Interdecadal Pacific Oscillation (IPO) [48]. During floods water salinity can fall to 5 ppt, while drought conditions can produce salinities of 45 ppt [57].

Seagrass beds (*Zostera capricorni*, *Halophila ovalis*, *Ruppia megacarpa*) are distributed around the margins of the lake today, whereas prior to recent urban development of the lake catchment, seagrass also occupied the centre of the lake [30]. Polychaetes and bivalve communities dominate macrobenthos and vary in composition according to the substrate type. Much of the immediate catchment has been cleared for urban development, leaving only residual areas of closed forest, scrub, sedgeland/grassland and open heath [57]. The rock units surrounding and underlying Tuggerah Lake comprise sandstone, siltstone and shale of the early Triassic Narrabeen Group and the mid-Triassic Hawkesbury Sandstone [59].

2.2. Core collection

Sediment cores were collected at two sites; core PI was collected from the distal margin of the flood-tide delta, immediately south of Pelican Island, while core CB was collected on the southern margin of the Ourimbah Creek bay-head delta in Chittaway Bay (Fig. 1). Cores were collected in 90 mm diameter, 6 m long plastic tubes, pushed into the sediment using a hammer system. At site PI the core barrel penetrated to 434 cm (534 cm below sea level) before meeting excessive resistance associated with penetration of Pleistocene stiff clay. At site CB, only 251 cm of sediment penetration was achieved (331 cm below sea level), reflecting the shallower location of the Holocene–Pleistocene boundary at this site. Cores were returned to the laboratory (University of Technology, Sydney) where they were split vertically for sub-sampling and lithological description. Subsequently, all cores were stored frozen to minimise sediment alteration.

2.3. Magnetic measurements

Magnetic sub-samples (8 cm³) were collected every two centimetres and analysed immediately (to prevent time-dependent sample alteration) for low- and high-frequency magnetic
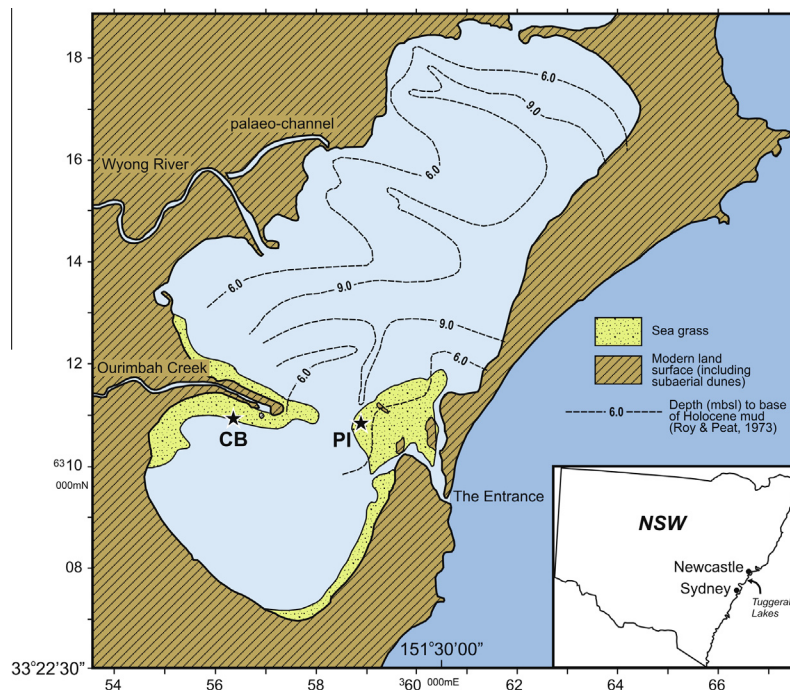
Fig. 1. Map of Tuggerah Lake (NSW, Australia) showing the two study site locations (starred) where sediment cores were taken; Chittaway Bay (CB) and Pelican Island (PI). Black-dotted areas indicate the location of *Zostera muelleri* seagrass.

susceptibility (χ_{LF} and χ_{HF}) using a Bartington MS2B dual-frequency sensor. Samples were then stored at $-5\ °C$ prior to the analysis of isothermal and anhysteretic remanent magnetisation (IRM and ARM) at the CSIRO magnetic laboratory at North Ryde. The ARM (acquired using a 100 mT alternating field with a 79.6 Am^{-1} bias field) and IRM (acquired using a 1T pulsed field) measurements were performed on a 2G cryogenic magnetometer positioned within a low-field environment. The interpretation of the magnetic data was supported by SEM (Philips XL30 SEM with Oxford ISIS EDS) and TEM (JEOL JEM-1200EXII TEM) images of magnetic separates collected from a recirculating system that pumps a water/sediment slurry (<63 μm fraction) past two NdFeB magnets.

2.4. Geochemistry

Samples for major and trace element geochemistry were collected every 5 or 10 cm in core PI and every 10 cm in core CB. Samples were oven dried at 60 °C overnight and then ground to a fine powder. For the PI core, analyses were performed on a Philips 1404 WO-XRF spectrometer (University of Newcastle) using fused beads with a sediment:flux ratio of 1:5. For the CB core, analyses were performed on a Spectro X'Lab 2000 Polarised EO-XRF (University of Newcastle), using a fused bead for the major oxides and a pressed pellet for the trace elements.

2.5. Grain size

Grain size analysis was performed using a Malvern Mastersizer/ E set (1.2–600 μm range setting) at the University of Technology Sydney (UTS). Approximately 2 cm^3 of wet sample was collected every 10 cm and washed briefly with a hydrogen peroxide solution to disperse faecal pellets. Larger shell fragments and organic fragments were removed at this stage. Samples were then washed through a 500 μm sieve into the Mastersizer dispersion tank. Sediment retained in the sieve was dried and then further characterised using 707 μm and 1000 μm sieves. The sieve data was then combined with the Mastersizer results.

2.6. Radiocarbon dating

Conventional and AMS radiocarbon dating was carried out at the Waikato Carbon Dating Laboratory (University of Waikato, New Zealand) and at the AINSE AMS facility at Lucas Heights, Sydney. Conventional dates were obtained from bulk mud samples collected at lithological and magnetic boundaries (the latter defined by abrupt changes in the magnetic susceptibility characteristics); these initial results were supplemented by twelve AMS^{14}C dates on whole shells and wood/charcoal fragments collected at various depths in both cores. Calibration of the radiocarbon dates was performed with Oxcal3.10 using the calibration curves shCal04.14c for the wood and charcoal samples and Marine04.14c for the shell samples; in the latter case, a local correction of 3 ± 70 was applied. We have used the same calibration curves to match those used by Roy and Thom [54]. Table 1 provides information about each sample that was age dated. Several samples (three from PI and one from CB site) gave age dates that were inconsistent with the age model. These inconsistent dates were not associated with any bioturbation features; however, grain size and geochemical data (see below) suggest that these inconsistent dates were caused by reworking of tidal-delta sand at the PI site and delivery of old organic matter by the river at the CB site.

3. Results

3.1. Lithostratigraphy

Both cores have a tripartite lithostratigraphy (Fig. 2), consisting of an upper muddy sand unit (unit 1), a sandy mud unit (unit 2), and a basal clay unit (unit 3). The top 10 cm of the cores contained seagrass fragments, roots and a larger proportion of mud. In the PI core, unit 1 has a yellow hue (7.5Y 4/4), varies from fine- to coarse-grained sand and is heavily bioturbated; the mud-lined *Skolithos* burrows are clearly defined. In unit 1 of the core CB, the transition between the sandy mud and muddy sand units is located between 115 and 85 cm, with a gradual increase in a grey-hued (9Y 3/5), medium grain-sized sand component. A small cluster of broken and whole shells occurs at the base of the unit, with only a minor content <2% of shell fragments above this point. Bioturbation in the muddy sand unit is extensive, producing poorly preserved ichnofabrics in which the mud component produces a mottled appearance; mud occurs dominantly as faecal pellets. Small, sand-sized fragments of charcoal are dispersed throughout, with occasional larger fragments.

In both cores, the sandy mud unit 2 (411–210 cm in PI: 244–100 cm in CB) is largely a drab, grey to olive-grey (1 GY 3/2) unit with a varying content of whole and fragmented shells; the shell

Table 1
Results of radiocarbon 14-carbon age dating.

Core sample code	Laboratory sample code	C^{14} age	Error	Calibrated ages (year BP)	2σ error	Depth (cm)	Material	Lab	Comment
Pelican Island									
PI225	Wk-12464	6670	60	7500	90	225	Wood/charcoal	Waikato	Not used in age model
PI231	Wk-8741	3170	250	3350	580	231	Mud	Waikato	Not used in age model
PI243	Wk-13401	2260	50	1880	200	243	Shell	Waikato	
PI247	Wk-12465	4560	50	5180	80	247	Wood/charcoal	Waikato	Not used in age model
PI318.5	OZG208	2990	40	3100	110	318.5	Wood/charcoal	ANSTO	
PI328	Wk-10406	3650	100	3550	280	328	Shell	Waikato	
PI347.5	OZG209	4130	40	4670	130	347.5	Wood/charcoal	ANSTO	
PI364.5	Wk-8742	5840	330	6650	670	364.5	Mud	Waikato	
PI374	OZG211	7780	50	8560	110	374	Wood/charcoal	ANSTO	
PI404	Wk-8743	8130	160	9000	400	404	Mud	Waikato	
Chittaway Bay									
CB107	Wk-12461	1100	50	980	110	107	Wood/charcoal	Waikato	
CB108	Wk-8744	1860	230	1800	110	108	Mud	Waikato	Not used in age model
CB117	Wk-13391	1640	50	1470	120	117	Wood/charcoal	Waikato	
CB172	Wk-12462	2369	50	2380	180	172	Wood/charcoal	Waikato	
CB213	Wk-16725	3354	40	3190	210	213	Shell	Waikato	
CB229	Wk-10407	3950	70	3950	230	229	Shell	Waikato	
CB242	Wk-8745	5300	200	6000	240	242	Mud	Waikato	
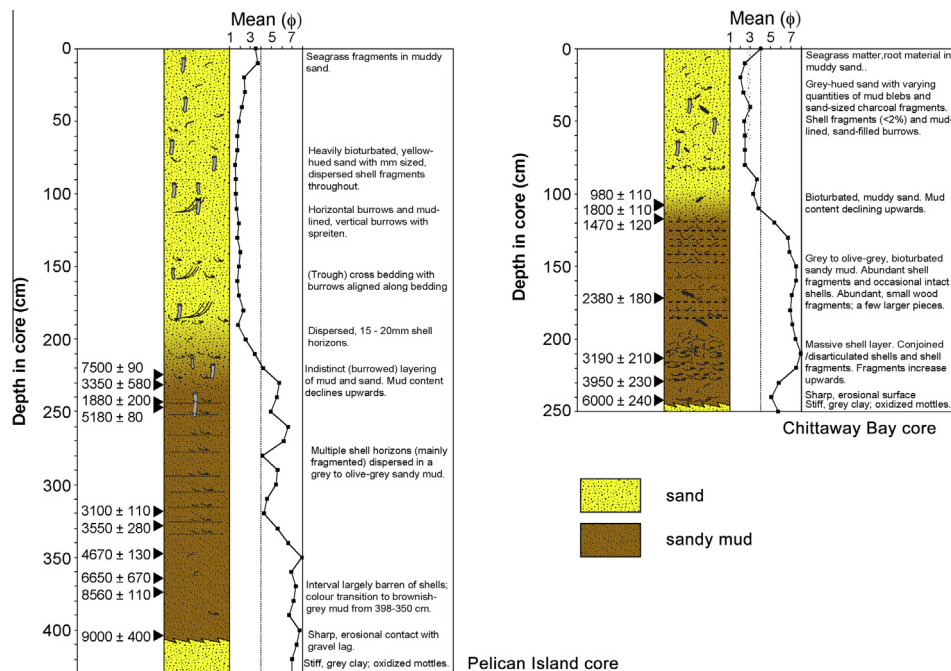
Fig. 2. Lithostratigraphy of sediment cores from Pelican Island and Chittaway Bay (Tuggerah Lake, NSW, Australia) showing variation in mean grain size, shell assemblages, and calibrated ages. A description of sedimentary and bioturbation features is provided in the right hand panel.

assemblage is dominated by the bivalve *Notospisula trigonella*, with rare occurrences of the gastropod *Nassarius jonai*. In CB, shells are present throughout most of the unit, but with notable shell accumulations occurring between 229–197 cm. 183–180 cm. 178–175 cm. 168–163 cm, 138–132 cm. 126–119 cm and 108–102 cm. Most shells are disarticulated, many fragmented, and the proportion of fragmented shells increases upwards. The most significant shell accumulation in CB (229–197 cm) is characterised by an abrupt base, a more diffuse upper-boundary, larger shells towards the base and an increasing proportion of shell fragments towards the top of the deposit. The overlying shell layers contain a large proportion of fragments and some contain large fragments (up to cm-scale) of wood and/or charcoal. In the PI core, the lower 75 cm of unit 2 are almost barren of shells, with the exception of one juvenile conjoined specimen of *Notospisula* at 388 cm and one or two small shell fragments above that point. The interval 398–350 cm shows a colour transition from olive-grey, to brownish-grey (9.7Y 4.5/4; most apparent between 394 and 374 cm) and back to olive-grey. Accumulations largely composed of shell fragments occur between 359 and 356 cm. 349–332 cm (also a few complete *Notospisula* valves and gastropod shells), 323–320 cm. 301–297 cm. 294–291 cm and 288–284 cm: the interval between 280 cm and the top of unit 2 has shell fragments disseminated throughout, with rare intact individuals near the top of the unit, including pyritized specimens of *Ammonia beccarii*.

Wet sieving of samples for grain-size analysis shows that the sand fraction in unit 2 of both the CB and PI cores is dominated by sub-rounded to sub-angular quartz grains, with a minor lithic component (<2%). Part of the quartz fraction shows iron staining, giving an orange hue (6Y 6/7) to the sand in the lower part of the unit. This iron staining is lost by 170 cm in CB1 and by 340 cm in PI, with the sand above these levels assuming a greyish hue (9Y 8/2). In core PI, the uppermost part (245–205 cm) of the sandy mud unit contains long (~20 cm), vertical sand-filled burrows. This interval represents the transition to the upper muddy sand unit (unit 1) that starts between 200 and 190 cm.

In both cores, unit 3 (434–411 cm in PI, 251–244 cm in CB) contains fine quartzose sand and lithic fragments and is discriminated from unit 2 on the basis of colour and competency, rather than texture. The clay in CB is grey (1 GY 7/2) with oxidised patches (6Y/R 6/7); it is sticky to the touch and can be readily moulded. In PI the basal 8 cm appear identical to the clay in CB, but from 426 to 411 cm the clay becomes dominantly oxidised (7Y 4/5.S), with grey mottles and dispersed fragments of black organic matter. In the CB core, we have only the soil C horizon, which in both cores shows colour variation consistent with gleying. In addition, the PI core has a partial soil B horizon, with organic fragments that may be root material. In both cores, the contact between unit 3 and 2 is irregular; core PI shows an accumulation of angular ironstone fragments and small pebbles immediately above the contact (411–408 cm: 6.7Y 4/3) whereas in the CB core the contact is overlain by an accumulation of shell fragments that show evidence of significant dissolution.

3.2. Grain size

The down-core grain size variation is presented in Fig. 3 as sand–silt–clay percentages, with the phi-size volume distribution shown for selected samples. All samples displayed a minimum of two grain-size modes (e.g. PI 000), with the majority having poly-modal distributions (e.g. PI 230). Each sample analysed corresponds with material taken from a ~1 cm slice; in chronological terms, 1 cm represents between 10-years (unit 1) and 100-years (unit 2) of accumulation and polymodal samples are therefore expected.

The flood-tide delta sediment of PI unit 1 is characterised by a well-sorted, coarse to medium sand (modal size 1.2–1.6 ϕ; see samples PI 000 and Pl l00 in Fig. 3), whereas the bayhead delta sand of CB unit 1 is a well-sorted, medium to fine sand (modal size 2.1–2.3 ϕ; see samples CB 000 and CB 040 in Fig. 3). These characteristic flood-tide and bay-head delta sands also occur, respectively, within samples PI 320 and CB 230. In CB, the majority of unit 2 is dominated by clay and silt components, with minor contributions
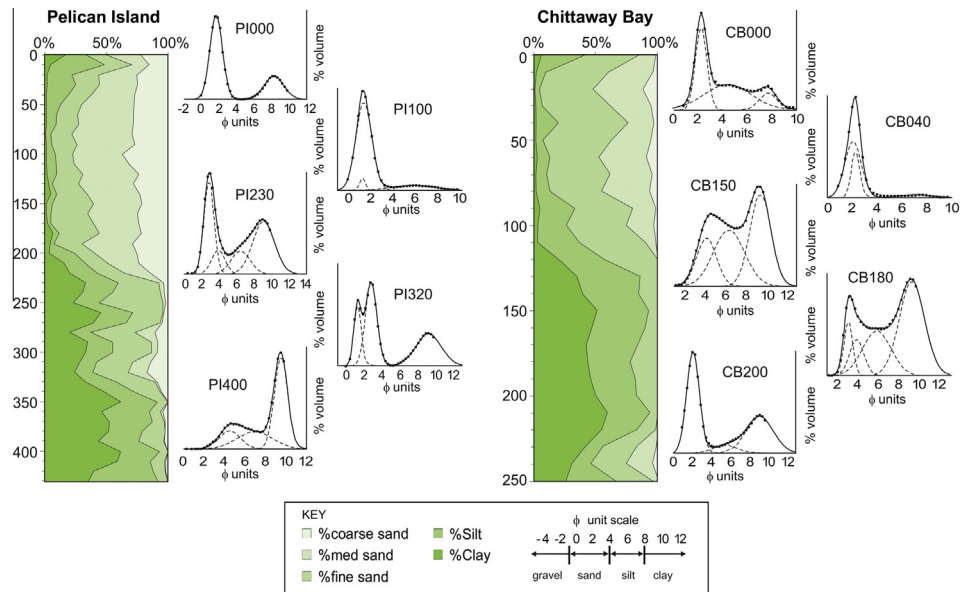
Fig. 3. Down-core variation in sediment grain size classes for cores taken from Pelican Island (PI) and Chittaway Bay (CB) (shaded, left hand panels). Selected representative grain size distributions shown in graphs on right side of each core. The presence of polymodal grain-size distributions in the samples is consistent with changing modes of deposition and the potential for both fluvial and marine contributions, with the dominant mode switching between coarse grain size in the upper half of both cores and fine grain size in the lower half.

from fine to very-fine sand, but there is a clear increase in the medium sand content at the base of the unit (below 230 cm; ∼4000 cal. years BP). In core PI the lower part of unit 2 (below 335 cm: ∼3800–9100 cal. years BP) is texturally similar to the main part of unit 2 in core CB (225–125 cm; ∼3600–1600 cal. years BP). However, the upper part of unit 2 in core PI (above ∼335 cm; ∼3800 cal. years BP) fluctuates between sandy mud and muddy sand (influxes of sand centred at 315 cm, 280 cm and 250 cm) and shows reduced silt content in comparison to unit 2 of CB.

3.3. Magnetic properties and electron microscopy

The down-core behaviour of the concentration-dependent magnetic parameters (χ, SIRM, ARM) and interparametric ratios (χ_{ARM}/χ, ARM/SIRM and SIRM/χ) are summarised in Fig. 4, accompanied by the down-core variation in mud content <63 μm sediment fraction). For the PI core, the ARM/SIRM plot comprises two data sets; the first obtained shortly after the core was collected and the second obtained after four years of cold (∼4 °C) storage. Both PI data sets show a remarkable degree of consistency (a scatter plot of the two data sets yields a slope of 1.02 with an r^2 value of 0.91), which suggests that cold storage was an effective means of minimising the alteration of remanence-bearing ferrimagnets in the PI core.

In both cores, the χ data provide a 3-fold subdivision of Holocene sediment; χ values drop significantly from the core maximum values that are achieved in the lowest ∼60 cm of Holocene sediment and then decrease again with the change from a mud-dominated to sand-dominated lithology at the unit 2/unit 1 boundary. This pattern in the χ data is to some extent replicated by the variation in the mud content of both cores, implying that the change in χ values is driven by underlying lithological change. The remanence (ARM and SIRM) data show an equally abrupt reduction in magnitude at the lower χ boundary, but a relatively small change accompanies the unit 2/unit 1 transition. The interparametric ratios indicate the nature of the change at the lower magnetic boundary; increased values of ARM/IRM and χ_{ARM}/χ indicate that the basal Holocene sediment is dominated by an ultrafine ferrimagnetic component that is absent from the remainder of

the unit-2 sediment. The enhanced ARM/SIRM values of this component are consistent with published values for intact chains of magnetosomes [42].

High ARM/SIRM values are present within two regions of unit 1 in the PI core, although the values are somewhat lower than in the basal Holocene sediment, implying that magnetosomes exert a lesser influence on magnetic parameters than is the case at the base of unit 2. The presence of magnetosomes in the high ARM/SIRM regions of both unit 1 and unit 2 was confirmed by TEM images (Fig. 5) obtained from magnetic separates. Equant magnetosomes are dominant, occurring often as intact chains; with occasional teardrop-shaped examples also observed. SEM images from CB samples (Fig. 5) indicate the presence of euhedral and framboidal pyrite within both the weakly (112 cm) and strongly (230 cm) magnetic unit-2 sediments. None of the pyrite framboids exceed a diameter of 12 μm, and some framboids appear to be partly infilled; euhedral pyrite is consistently less than 5 μm in size and is the more common form of pyrite in these samples.

In the CB core, the ARM/SIRM ratio suggests little change in the character of the remanence-bearing ferrimagnets in the upper 178 cm of the core. However, the SIRM/χ and χ_{ARM}/χ ratios show a distinct increase in values that starts at ∼130 cm, within the upper part of unit 2. This different behaviour of ratios involving χ can be explained by an upward-decreasing paramagnetic contribution (provided by clay and/or pyrite) or by a decrease in the relative contribution of SP-sized ferrimagnets. The inverse correlation of SIRM/χ with the mud content (Fig. 4) suggests the influence of a paramagnetic clay component. In the Pleistocene clay, the concentration-dependent parameters indicate a magnetic content that is similar in magnitude to the equivalent Holocene material, whereas the interparametric ratios indicate a much-reduced proportion of ultra fine magnetic particles. The sharp peak seen near the base of the PI core corresponds with the ironstone fragments that occur at the Holocene–Pleistocene boundary.

The IRM acquisition data for selected samples are shown in Fig. 6. Samples from the basal Holocene sediment (CB 200; PI 362), dominated magnetically by magnetosomes, exceed 90% of their saturation value following the 100 mT-acquisition step. Conversely, the samples from the magnetically coarser regions (CB 88;
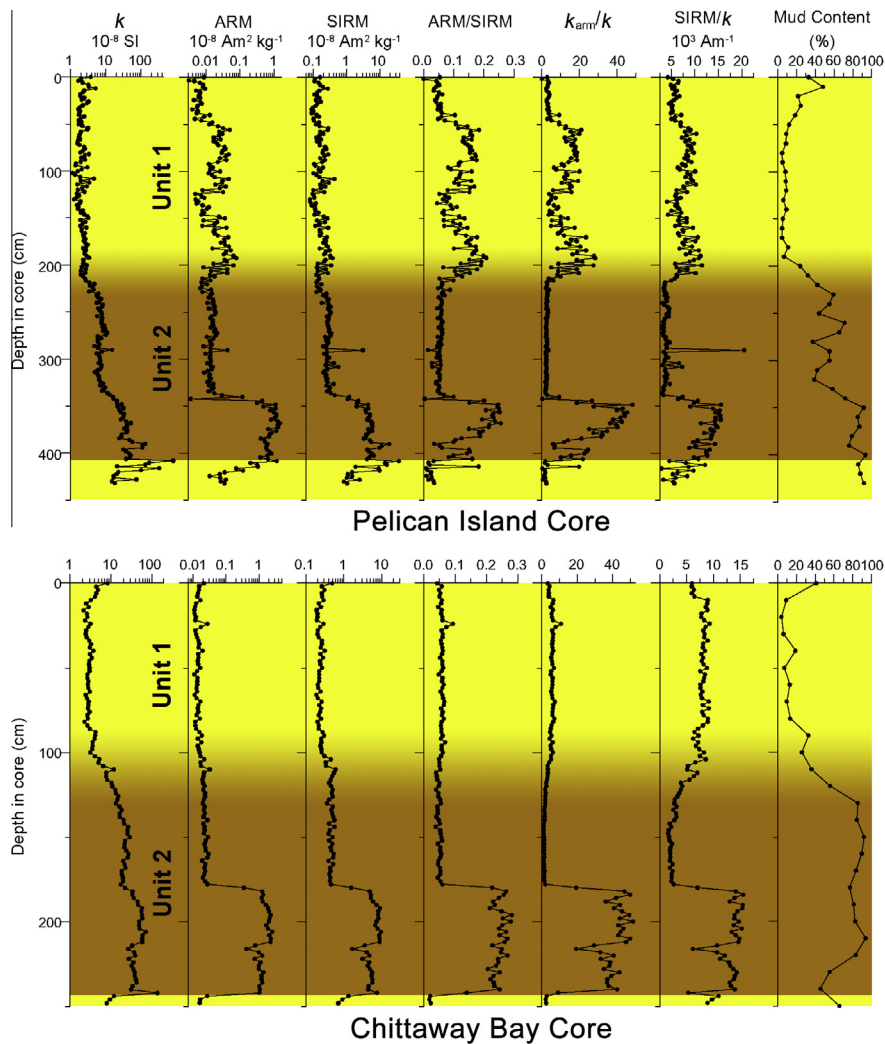
Fig. 4. Magnetic properties of estuarine sediment cores from Pelican Island and Chittaway Bay in Tuggerah Lake (NSW, Australia). Shading indicates lithostratigraphic subdivisions as shown in Fig. 2. While magnetic susceptibility (*k*) shows a distinct relationship with mud content, those parameters and interparametric ratios that are sensitive to magnetic grain-size show a more complex signature that can be linked to variations in the contribution from bacterially generated ferrimagnetic material. Single domain minerals are most common in sediments immediately overlying the Holocene transgression surface, but are abruptly replaced by ferromagnetic material towards the top of Unit 2. In the case of the Pelican Island core, this can be equated with the first influx of fluvial derived muds at ~2700–2400 cal year BP. Our interpretation is that although muddy sedimentation remained dominant until ~1500 cal year BP, the replacement of single domain grains by ferromagnetic material at ~2500 cal year BP heralded the first influx of fluvial material at this time (see discussion in text).

CB 140; PI 280) show a more gradual increase in IRM at lower applied field and acquire ~20% of their total IRM at fields above 100 mT. The sample taken from one of the upper zones of increased ARM/SIRM values in the PI core (PI 180) shows behaviour intermediate between these two patterns; IRM acquisition occurs initially at a rate similar to that displayed by the magnetosome-dominated samples, but by 100 mT the behaviour of PI 180 is identical to the magnetically coarser samples.

Thermomagnetic data from bulk samples (Fig. 7) indicates that the zones of high ARM/SIRM in the PI core are dominated by a ferrimagnetic component with a Curie temperature close to 600 °C (PI 70; PI 190) which, after heating, is reduced in magnitude. However, the Curie curves of samples from PI unit 2 (PI 250; PI 350; PI 400), irrespective of the sample ARM/SIRM value, are dominated by the formation of a ferrimagnetic phase that is initiated at ~400 °C, behaviour that is consistent with the oxidation of pyrite to magnetite [66]. The Curie curves of two magnetic separates (CB 170; CB 190; Fig. 7) helps to discriminate the ferrimagnetic mineralogy of unit 2 samples. Sample CB 190 was collected within the zone of high ARM/SIRM values at the base of CB unit 2, while CB 170 was

collected from immediately above the same zone. In CB 170, the heating curve shows an inflection with a major decrease in magnetisation between 350 °C and 450 °C and a Curie temperature (T_C) of ~620 °C. On cooling, the ~620 °C Curie temperature is retained while the inflection seen in the heating curve is lost and the room temperature magnetisation is reduced by ~80%. In contrast, sample CB 190 shows a smaller decrease in magnetisation on heating up to 450 °C, after which the magnetisation decreases abruptly and provides a Curie temperature of ~590 °C. On cooling, the ~590 °C Curie temperature is retained, the minor inflection seen in the heating curve is lost and the room temperature magnetisation is reduced by ~35%.

The change in magnetisation seen below 450 °C in both heating curves, together with the considerable loss of magnetisation after heating, are compatible with published thermomagnetic curves for fine-grained maghemite [16], where the decrease in magnetisation results from the inversion of maghemite to haematite. Maghemite is the most commonly formed ferrimagnetic mineral during pedogenesis [56] and we consider that it represents primary catchment input. In the case of CB 190, the thermomagnetic data
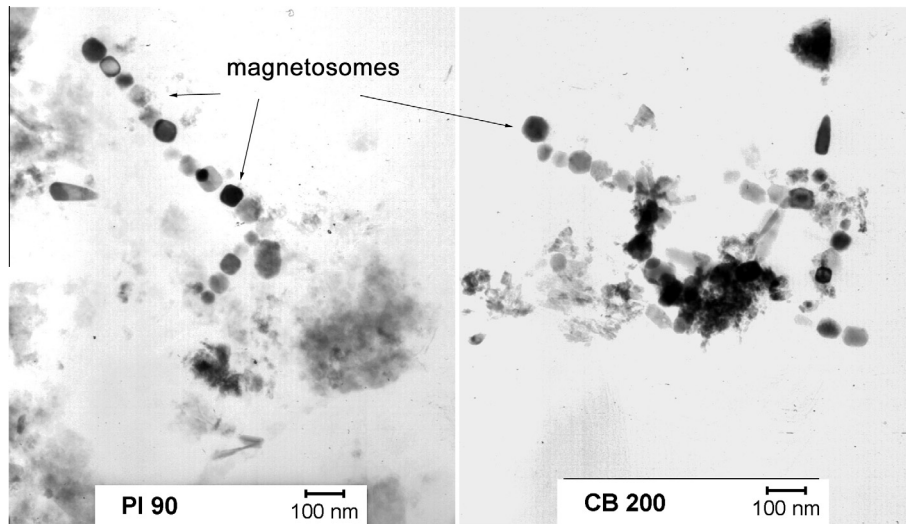
Fig. 5. Transmission electron microscope (TEM) showing the presence of single-domain magnetosomes in Pelican Island (PI) and Chittaway Bay (CB) cores from Tuggerah Lake (NSW, Australia). Intact chains of equant magnetosomes are observed in both TEM images, together with isolated, teardrop-shaped examples.
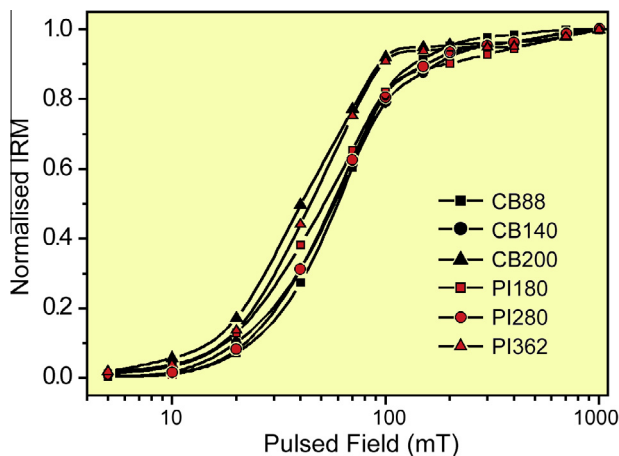
Fig. 6. Isothermal remanent magnetisation (IRM) acquisition data for selected samples (depths) taken from Pelican Island (PI) and Chittaway Bay (CB) sediment cores. Acquisition curves can be interpreted in terms of the presence of two magnetic phases. The difference in the shapes of the curves for PI362 and CB200 confirm the paramagnetic origin of the magnetism seen in the lower sections of the two cores.

suggest the presence of an additional, magnetite phase, which we ascribe to the bacterial magnetosome component identified in the TEM images (Fig. 5) and inferred from interparametric magnetic ratios (Fig. 4). Greigite magnetosomes, which are synthesised by magnetotactic bacteria under sulphidic conditions [38], would be identified through decomposition on heating above 200 °C [65].

We therefore have evidence that diagenetic pyrite and single domain magnetosomes coexist in the basal Holocene sediment of CB, indicators of sulphidic (anoxic) and sub-oxic conditions, respectively. As noted above, the bulk samples PI 70 and PI 190, taken from the upper zones of enhanced ARM/SIRM values, also display magnetite Curie temperatures; these PI samples lack, however, clear evidence of the maghemite phase that undergoes inversion during the heating of CB 190. We believe that this lack of maghemite in the PI 70 and PI 190 samples, both of which come from the sandy flood-tide delta unit, is consistent with fluvial delivery of the maghemite component seen in the unit-2 samples.

In summary, the ferromagnetic content of both cores is provided by one or both of two components; maghemite, derived from

the catchment soil profile, and SD-sized authigenic magnetite generated by assimilatory microbial processes. Lithic fragments do not appear to make a significant contribution to the core magnetic properties (except within the lag layer of the PI core), consistent with the dominant supply of coarser material from the sandy Triassic units.

3.4. Geochemistry

3.4.1. Major oxides

The down-core variation of the major oxides is shown in Fig. 8, with all data normalised to the average shale value [67,69]. As a reference for the sandy units, in each graph we also plot (as a vertical line) the equivalent value obtained from sandstone geostandard GSR-4 [26], normalised to the average shale value. The horizontal broken line in the PI data represents a significant textural boundary, with a large increase in the sand content between 350 and 320 cm (see Fig. 3); this boundary is used to subdivide unit 2 for the purposes of the CVA analysis (see below). Where a graph has missing data points, this reflects samples (depths) for which the particular oxide was below the detection level of the XRF instrument.

The pattern of variation in the major oxides is dominated by a marked shift associated with the transition from the sand-dominated unit 1 to the mud-dominated unit 2. In broad terms, the trend displayed by SiO_2 is in anti-phase with the trends of the other major oxides (except CoO; see below). The geochemical data provide an example of compositional, or 'closed' data (data, which sums to unity, or to 100%; [1], in which interdependence is inherent between the compositional parts (here major oxides) of each sample.

3.4.2. Trace elements

In both cores, the pattern of variation displayed by the majority of the trace elements broadly correlates with the down-core behaviour of the Al content, consistent with the known linear relationship between trace element content and the fine-grained component of sediments (e.g. [17]). Exceptions are Sn (PI core) and Se and Ge (CB core), which instead correlate with the behaviour shown by SiO_2 In addition, in both cores CaO and Sr content strongly covary, indicating that both are mainly derived from the shell content. Therefore, down-core trends in major oxides and
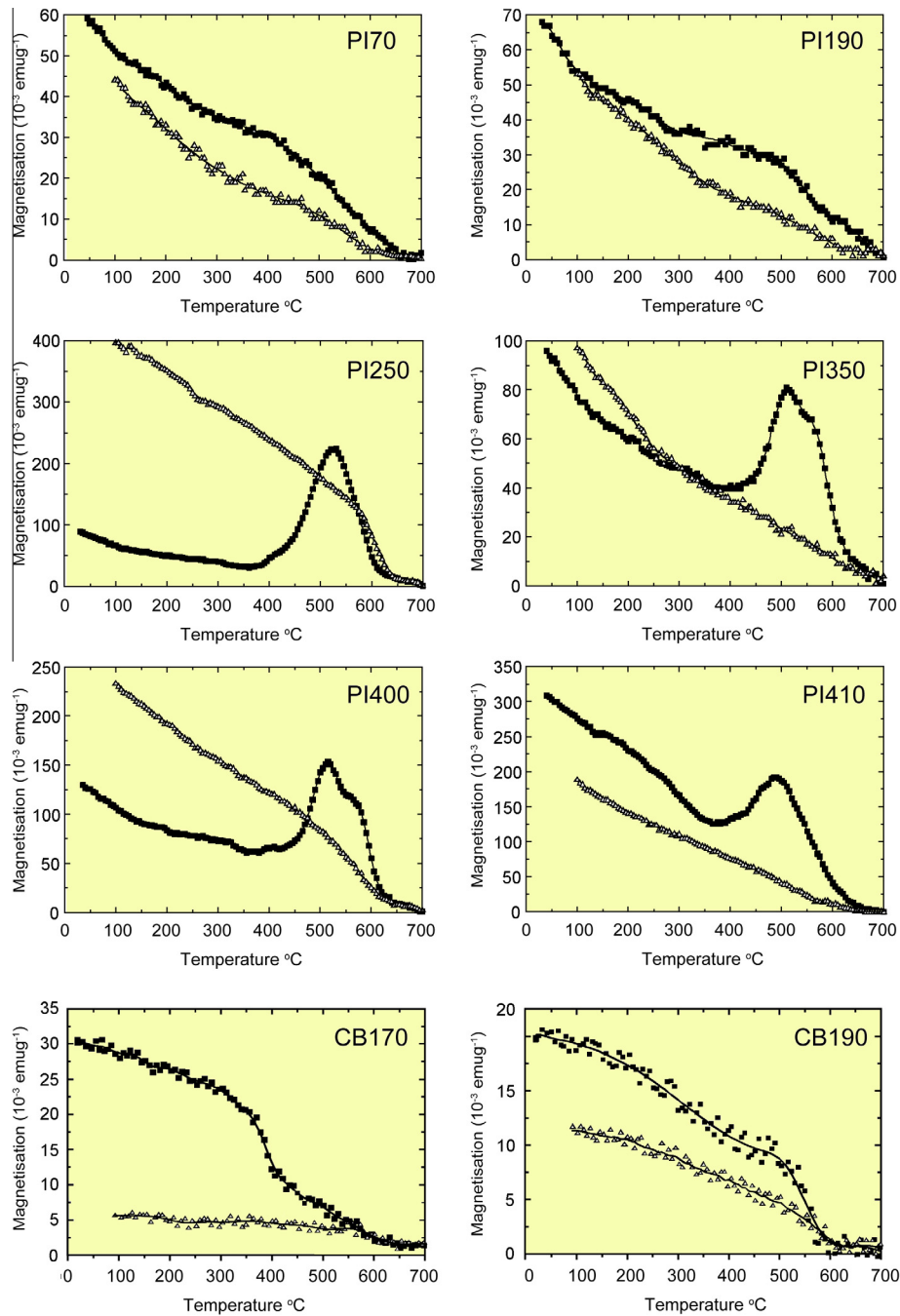
Fig. 7. Thermomagnetic data from bulk samples taken from Pelican Island (PI) sediment cores. Heating curves (solid symbols) for the four deeper samples show the generation of a ferrimagnetic phase when the temperature exceeds ~400 °C; this new phase is retained on cooling.

trace elements mainly reflect changes in sediment grain-size and provenance (marine versus fluvial), with some additional variation provided by authigenic and redox-related effects (see below). The presence of ironstone nodules at the unit 2/unit 3 boundary in the PI core produces extreme values of Fe_2O_3 in the sample taken from 410 cm. Analysis of a separated nodule gave a Fe_2O_3 content of 42%.

3.4.3. Geographic variability

Based on the location of both sites, supported by their lithostratigraphy and grain-size data, we expect that units 1 and 2 at the CB site are dominated, respectively, by fluvial-sand and fluvial-mud components, whereas at the PI site, unit 1 is dominated by marine sand and unit 2 comprises fluvial mud with an

upward-increasing contribution from marine sand. To determine whether this simple model is supported by the geochemical data, we have applied canonical variates analysis (CVA) to the major oxide data from the CB core. We excluded CaO and NaO_2 from the analysis because of, respectively, the influence of shell content and salt (some samples showed salt crystals after drying), factors that do not reflect clastic sediment supply. To obviate the constant sum constraint (data sum to 100%; [1], the data was transformed prior to analysis using the centred log-ratio transformation (CLR; [1]).

The CB and PI sample scores for the two canonical variates are shown as a bivariate scatter plot in Fig. 9, with PI unit 2 subdivided into two sub-units (Fig. 8); 220–335 cm (unit 2a) and 340–385 cm (unit b). CVA has readily separated the CB samples into the three
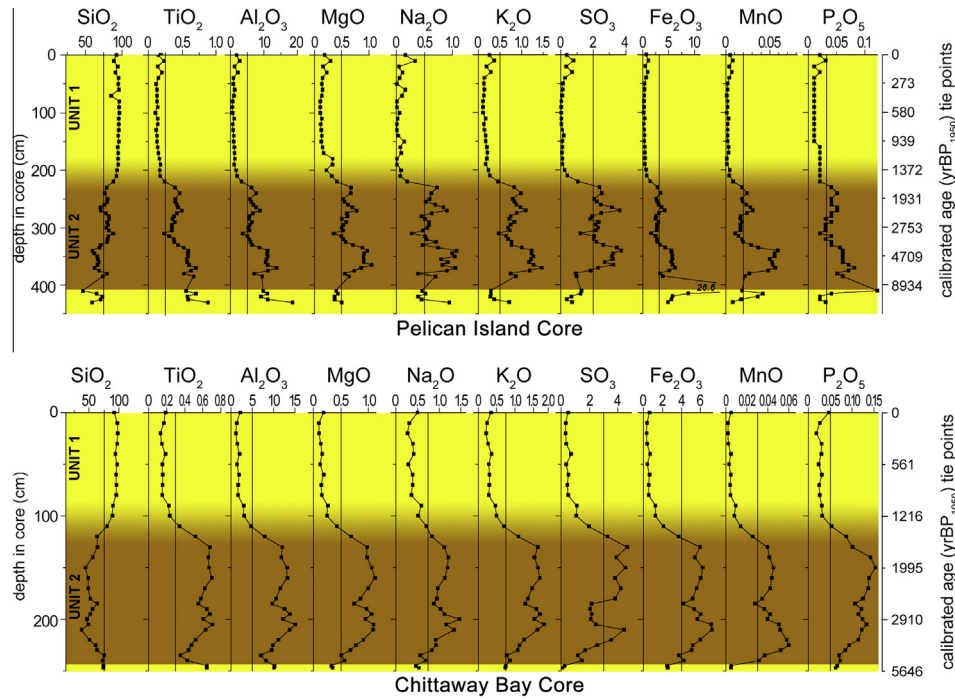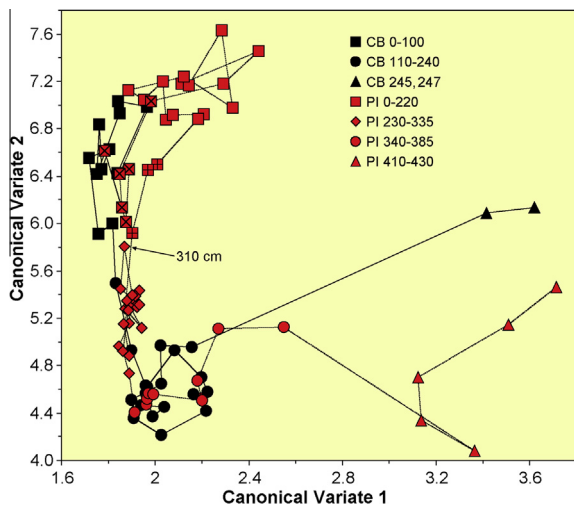
Fig. 8. Down core variation in the weight percent of major oxides within sediment cores from Pelican Island (PI – upper panel) and Chittaway Bay (CB – bottom panel) sediment cores. With the exception of SiO_2, the pattern of variation is directly related to mud content; SiO_2 is inversely related. The distribution of elements shown supports the 2-fold subdivision of the sequence into an upper unit (dominated by SiO_2) and a lower unit dominated by fine-grained aluminosilicates (Al_2O_3, MgO, K_2O). Additionally, the distribution of SO_3, Fe_2O_3 and MnO further supports the switch from a single-domain paramagnetic subunit of Unit 2, to fluvially derived clays, preceding the influx of coarser-grained sediment.

lithological groupings (units). Importantly, the plotting position of the samples from 90, 100, 110 and 120 cm suggest a geochemical trend between units 2 and 1, consistent with the gradual change in sediment character observed in the core. The location and within-in-group scatter of the PI data are very informative. The two basal unit-3 samples (425 cm; 430 cm) plot close to the two CB unit-3 samples, consistent with our interpretation that the bases of both cores represent a soil C horizon (gleyed Pleistocene clay). Although the majority of the PI unit-2b samples plot within the cluster of CB unit-2 samples, an observation that supports the geochemical

Fig. 9. Canonical variates scores for Chittaway Bay and Pelican Island (NSW, Australia). The canonical variates provide a means of sample discrimination, based on the major oxide content of the samples (with the exception of CaO and NaO_2). The process of discrimination attempts to assign to each sample the relative importance of each of two sediment sources.

similarity of these two groupings, the lower most unit-2b samples plot on a trend between the CB unit-2 samples and the unit-3 Pleistocene samples. The delineation of this trend is consistent with our earlier observation that the basal unit-2 sediment in the PI core (394–374 cm) has a brownish hue that is consistent with the inclusion of material eroded from the underlying unit-3, material that represents the upper part of the Pleistocene-early Holocene soil. Notably, the upper two PI unit-3 samples (415 cm; 410 cm) plot away from this trend, consistent with the grain-size and geochemical data which shows that the upper part of unit 3 has the highest clay and iron content for the core and may represent the remains of the soil B horizon (the sample from 410 cm also incorporates material from the lag deposit that sits at the unit 2/unit 3 boundary).

The two oldest unit-Z samples from the CB site also show a slight deviation towards the plotting position of the unit-3 samples, suggesting that the basal Holocene sediment at the CB site also includes a proportion of Fe-worked Pleistocene material. The majority of the PI unit-2a samples are clustered between samples CB110 and CB120 lone exception is the sample from 310 cm, which plots close to the margins of PI unit-l and CB unit-I; this sample corresponds to a layer of muddy sand, which has the lowest mud content of unit 2, and define a trend that runs subparallel to the trend between CB units 1 and 2. This trend suggests that the PI unit-2a samples contain a mixture of fluvial mud and fluvial sand. However, we note that the PI unit-1 samples plot close to the CB unit-l samples and therefore the location of the PI unit-2a samples might equally represent a mix of fluvial mud and marine sand; this seems the more likely interpretation because of the proximity of the PI site to the flood-tide delta. While the PI and CB unit-l sample groups show considerable overlap (some geochemical similarity between the fluvial and marine sand is expected, since both units are quartz-dominated and sourced, to varying degrees, from the Hawkesbury sandstone), the majority of the PI unit-l samples plot to the right of, and above, the CB unit-l samples. Where overlap of

the groups occurs, at the base and the top of PI unit-l, it can be ascribed to mixing of the marine sand with fluvial mud. To clarify this point, the samples from the top and the base of unit-l are marked with leaning- and upright-crosses, respectively. The slight offset between the CB unit-l grouping and the majority of the PI unit-l samples is mostly a reflection of a slightly increased K20 and AIP3 content in the former and slightly increased SiO$_2$ content in the latter, suggesting that the CB unit-l sand contains a minor feldspar component.

3.4.4. Redox conditions

A number of the oxides/elements are sensitive to redox conditions; their contribution to the initial fluvial or marine input can be modified in response to the location of the redox boundary and the consequent exposure of the oxide/element to oxic or anoxic diagenesis (e.g. [58,6,64]). Redox conditions respond to changes in water salinity and in the rates of clastic and organic sediment accumulation; therefore the redox-sensitive components provide supplemental information regarding these environmental variables. In Fig. 10, we show the down-core variation of the Al-normalised elements Fe, S, Mn, V, U, Cr, Ni. Cu, Zn, As, Mo and Se (the last two are not available for the PI core). Since a significant fraction of the trace element load to coastal sediments is delivered sorbed to clays, normalisation by Al content is used to compensate for variable sample clay content. Element enrichment is determined relative to the unit and by comparing our Al-normalised data with the equivalent Al-normalised value from the relevant geostandard; GSR-4 in the case of the sandy units (broken vertical line in Fig. 10) and the average shale value (solid vertical line) for the muddy units. These enrichment estimates need to be interpreted with caution, since enrichment may be primary (changes in the characteristics of the fluvial or marine source material) rather than secondary (produced by authigenic processes linked to sediment diagenesis). Secondary enrichment processes include the downward diffusion of elements from seawater and their immobilisation through valency change and/or sedimentation of organic matter enriched in trace elements through the process of bioaccumulation. A significant enrichment of trace elements by such redox reactions requires that the vertical location of redox boundaries

be maintained for a significant period of time, which requires slow, or intermittent, accumulation.

3.4.5. Iron diagenesis

Fig. 10 also shows the behaviour of %TOC, %S, %Fe and the ratios of Mn:Fe and Fe$_{av}$:S; the Mn:Fe plot also shows the relevant geostandard values as vertical lines, while in the Fe$_{av}$/S plot, the vertical lines represent the stoichiometric Fe:S ratio for iron monosulphide and for pyrite. If the bacterially-mediated reductions of Mn and Fe oxides are important processes within the sediment column, Mn reduction will occur at a higher redox potential and therefore precede Fe reduction. Liberated Mn^{2+} that diffuses upwards into the oxic zone will be precipitated as an oxide; liberated Fe^{2+} will also diffuse upwards, but may precipitate immediately below the oxic boundary through oxidation pathways involving nitrate or Mn-oxides [45,46]. The Mn:Fe ratio can therefore identify the depth at which the transition from oxic to anoxic sediment occurs. The ratio of iron to sulphur is used here as an indicator of the degree to which the available iron content of the sediments has been transformed to iron sulphide. The abiotic reduction of Fe-oxides by sulphide occurs within sulphidic sediments, where sulphide is produced during sulphate reduction, and within anoxic sediments when free sulphide is available through diffusion from the sulphidic zone (e.g. [3]). Here we use total sulphur as an indicator of iron sulphide content (assuming a minimal contribution from organic sulphur and other metal sulphide phases) and Fe$_{av}$ as an estimate of the proportion of reactive iron in the sediments that is available for bacterial reduction and/ or exposure to sulphide. The Fe$_{av}$ (reactive iron content) values are calculated using the sample Fe and Al content; the calculation assumes that the ratio Fe:Al in silicate minerals is ~1:4 and that the Al content of the sediments is exclusively retained within these silicate minerals [18]. The Fe$_{av}$ values are then obtained by subtracting from the total Fe content one quarter of the Al content.

In the PI core, the pattern of variation in Fe, S and TOC are strongly correlated, confirming the link between organic content and sulphate reduction and indicating that much of the iron in the core occurs as a form of sulphide. In the CB core, the Fe:S correlation is equally well developed, suggesting again that most iron
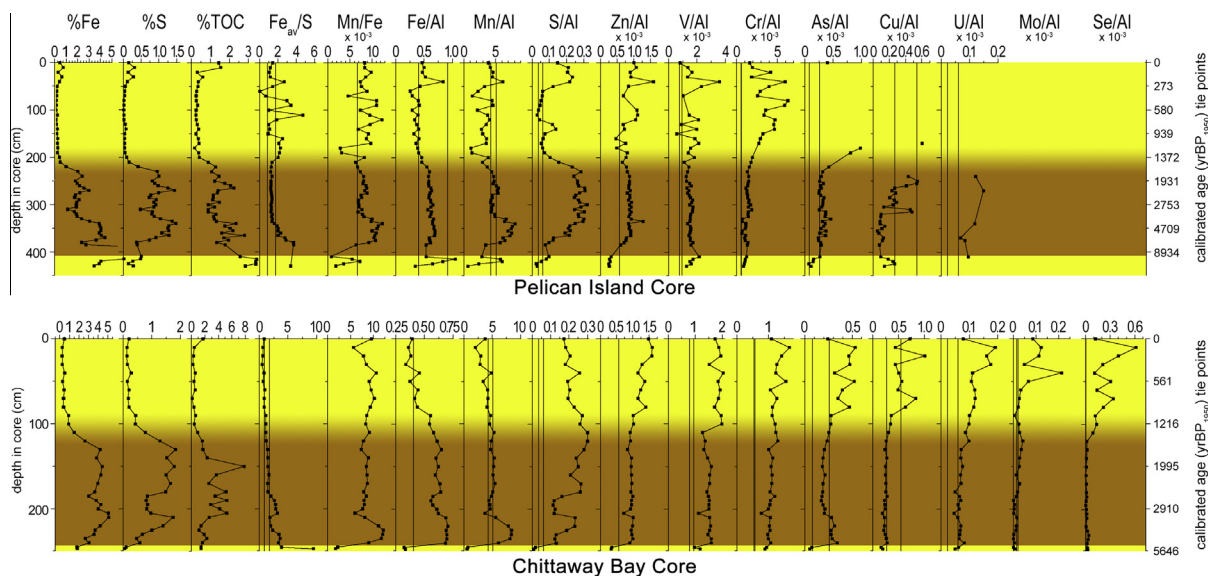
Fig. 10. Down core variation in the presence of selected major elements, total organic carbon and major element ratios within sediment cores from Pelican Island (top panel) and Chittaway Bay (bottom panel) sediment cores. Ratios of redox-sensitive elements (S; Fe; Mn) are used to infer the influence of changing redox conditions during the history of sediment accumulation in Tuggerah Lake. To compensate for varying mud content, Al has been used as a normalising factor for the majority of the elements.

occurs as sulphide. However, in the CB core the correlation of Fe and S with TOC is less certain; here the importance of terrestrial organic content is significant, as this poorly-reactive material does not readily drive sulphate reduction. The Fe/S plot has significance for the magnetic results: in regions of the core where the Fe/S value exceeds that of stoichiometric iron monosulphide (1.74), samples yield the strongest magnetic measurements (Fig. 4) and have inter-parametric magnetic ratios which indicate that single domain magnetosomes dominate the ferrimagnetic content (Fig. 4).

In the CB core, the Mn:Fe ratio exceeds the geostandard value (GSR-4; broken line in Fig. 10) for the majority of unit 1, suggesting that oxidising conditions dominated during the accumulation of unit 1. Oxidising conditions are supported by the presence of well-preserved agglutinated foraminifera, which use ferric iron cement to stabilise their tests [40]. The sample from 10 cm depth shows a local minimum in the Mn:Fe ratio; this sample occurs directly beneath the surface layer, which has an enhanced mud and organic content, and we interpret the decrease in the Mn:Fe ratio as reflecting the dissolution of Mn-oxides associated with anoxic conditions. Coincident with this Mn:Fe minimum, we see an abrupt decrease in the Al-normalised U, Cr. Ni, As and Se content, with the sample from the core top having the lowest Al-normalised values in unit 1. The increase in mud (and therefore Al) content is largely responsible for these decreases in Al-normalised values, but the behaviour of Se and U is consistent with *in situ* enrichment through the downward diffusion of these elements and their immobilisation below the oxic/anoxic boundary.

Of the redox-sensitive trace elements, only the Al-normalised As content replicates the preceding, broad maximum in the Mn:Fe ratio, while the %S data shows an upward increase through the equivalent section. The Mn:Fe minimum at 205 cm is replicated by Al-normalised values of V, U, Cr, Ni, Cu and Zn and coincides with the onset of a 25 cm zone of lowered %S values. The pattern of behaviour in redox-sensitive components below 200 cm (and including the zone of reduced %S values, which extends to 185 cm) suggests that post-depositional modification of the basal Holocene sediment has occurred; the behaviour does not appear to be significantly driven by lithological factors as it occurs independently of Al (or Si) content.

In the PI core, a 40 cm zone at the top of the core shows enhance levels of sulphur that correspond with an increased iron content and with increasing levels of organic carbon and mud (see Fig. 10). These data imply that an increased delivery of reactive iron and organic matter, probably due to catchment urbanisation, has lead to increased pyrite content within this zone. At the bottom of this zone, there are narrow peaks in the Al-normalised values of Fe, V, Cr. Zn and Mn; this pattern is consistent with the upward migration of reduced Fe and Mn species (and trace elements sorbed to the precursor oxide phases) and their immobilization at the oxic/anoxic boundary. Potential immobilization mechanisms in response to sediment and porewater anoxia include valency change and precipitation from pore-water (V, Cr; [6]) and precipitation as a sulphide phase (Fe, Zn; [41]). At 180–190 cm there is a zone of low Mn:Fe values (produced by an abrupt decrease in Mn) and enhanced As/Al values, located just above the unit 2/unit 1 transition. The abrupt decrease in Mn is consistent with the dissolution of Mn-oxides through exposure to reduced sulphur species diffusing upwards from the organic-rich unit 2.

3.4.6. Geochemical signature of provenance

In common with the CB core, the Mn:Fe ratio in PI unit 2 shows a distinct maximum in the lower part of the unit (380–325 cm). However, in the PI core this lower region of enhanced Mn:Fe values coincides with core-maximum values of organic matter, sulphide and Al-normalised Mn content while the other redox-sensitive trace elements do not show any significant change. This region of enhanced Mn content corresponds with the finest-grained section of the PI core; however, a major change in sediment provenance is not implicated because of the absence of a significant change in the other Al-normalised elements. Core-maximum pyrite content is indicated for this interval (note the Fe and S content; Fig. 10) implying that sulphate reduction is a significant factor. Consequently, alternative pathways for the enhancement of Mn content include the precipitation of a Mn-carbonate phase, as a response to the increased alkalinity that accompanies sulphate reduction [8,60], or the formation of a Mn-sulphide phase [60], a process that can occur in strongly-reducing sediments. However, Mn-sulphides ore favoured only when the supply of reactive iron is exhausted (Lepland and Stevens, 1998), which is not the case here. A narrow peak in the Al-normalised Cu content sits just above this region of pyrite-rich sediments; the peak occurs within a narrow interval (310–315 cm) that corresponds to the first significant influx of flood-tide delta sand at the site. Cu levels are low in the flood-tide delta sands of unit 1, suggesting that the Cu originates from the mud content; the enhanced permeability of the sandy layer at 310–315 cm may have acted to facilitate the downward migration of dissolved Cu. Precipitation of a Cu sulphide phase can occur when dissolved sulphide is present within the pore water [15]. At a higher level in unit 2, a second peak in Al-normalised Cu also coincides with a second layer of increased sand content, lending some support to this suggested mechanism.

4. Discussion

4.1. I Evolution of Tuggerah Lake

4.1.1. The early-to mid-Holocene sediment record (∼9000–7000 cal. years BP)

Our knowledge of the early Holocene comes only from the more seaward (PI) site, where wave ravinement has removed the soil A and (partial) B horizons and the Pleistocene–Holocene boundary at 407 cm is marked by a transgressive lag comprising ironstone nodules (of unknown origin). Here our oldest radiocarbon dates (Fig. 2) indicate that accumulation started at ∼9000 cal. years BP and that the sediment below 374 cm accumulated more rapidly than at any time prior to 2300 cal. years BP (sediment accumulation curve – Macreadie et al. under review). However, according to the sea-level model of Thom and Roy [63], any sediment accumulating at 9000 cal. years BP would have done so prior to marine flooding. This is illustrated graphically in Fig. 11, in which the PI age model (plotted as uncalibrated ages, for consistency with the model of Thom and Roy [63]) intersects with the sea-level envelope in the depth range 496–472 cm below sea level (396–372 cm core depth), equivalent to an age range ∼8900–8200 cal. years BP.

Our data indicate that significant changes in core properties occur at ∼380 cm (∼480 cm below msl; ∼8600 cal. years BP) because: (a) the geochemical data suggests that core material below 380 cm incorporates sediment that was reworked from the land surface (see Section 4.6); (b) there is a slightly increased sand content at 380 and 390 cm, which coincides with a diminished magnetosome component, with low values of manganese, iron and sulphur; (c) the first shell fragments appear at 380 cm; and (d) the sulphur content starts to increase rapidly above 380 cm. The sediment below ∼380 cm represents a mix of reworked soil material and contemporaneous sediment that was rapidly deposited following the transgression. The basal date of ∼9000 cal. years BP was obtained from a mud sample collected at a core depth of 404 cm; the date therefore reflects an average age of the reworked/fluvial mix and is consistent with the incorporation of plant material from the pre-flooding Holocene land surface. Supporting this interpretation, we note that sieving of the 380 cm
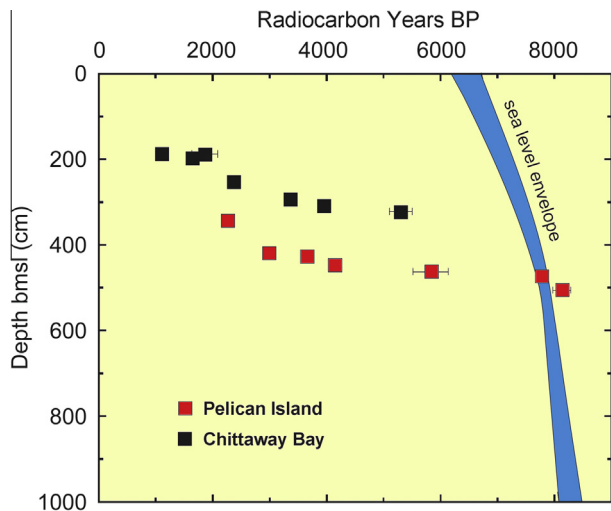
Fig. 11. Core sediment age (in radiocarbon years)-depth pairs from the Chittaway Bay and Pelican Island cores plotted against the sea-level envelope of Thom and Roy [63]. The Tuggerah data are consistent with sea-level flooding occurring after 9000 cal year BP.

sample yielded wood fragments and plant fibres. The origin of the contemporaneous sediment within the 380–390 cm interval appears different to the fluvial mud that dominates above; in terms of iron and manganese content, the geochemistry of the sample from 385 cm is significantly different to the samples immediately above, a difference that seems out of proportion with the slightly increased sand content. It is our view that this interval includes material reworked from a gleyed soil horizon, from which iron and manganese oxides had been removed by diagenetic processes.

The co-occurrence of pyrite and fine-grained (bacterial) magnetite in the basal Holocene sediments (extending to 344 cm) is unexpected. Pyritisation involves the abiotic reduction of iron (oxyhydr)oxides by contact with sulphide, where the reactivity of iron (oxyhydr)oxides to dissolved sulphide is directly proportional to specific surface area. Therefore, magnetosomes should be preferentially dissolved in comparison to detrital ferrimagnetic minerals. However, pedogenesis can produce significant quantities of amorphous iron (oxyhydr)oxides, the reactivity of which is one to two orders of magnitude faster than crystalline forms of iron such as magnetite [11,47]. A supply of pedogenic iron is consistent with the high iron content of the earliest Holocene sediments and is supported by our identification of maghemite in the muddy core intervals. Furthermore, we note that iron staining persists on the quartz grains within this earliest Holocene interval, but is absent from quartz grains above the zone containing magnetosomes, consistent with an excess of iron in the former interval. Consequently, we believe that the muddy basal Holocene sediment has sufficient amorphous iron (oxyhydr)oxides to exhaust the supply of sulphide and to provide a source of iron for magnetotactic bacteria.

The high Mn:Fe values found in much of the earliest Holocene sediment are also significant: if the high iron content of the basal Holocene sediments is derived from the erosion of the weathered Pleistocene clay that formed the land surface, then the high Mn levels could be similarly derived. However, we have argued that iron dissolution occurs within this core interval, which means that Mn dissolution is also favoured and should have preceded iron reduction, unless the Mn occurs as a detrital phase within lithic fragments. The dissolution and diffusion of Mn can produce high levels of authigenic Mn in the surficial (oxic) deposits of coastal sediments [7], particularly when accumulation rates are low. However, the retention of enhanced levels of authigenic Mn in the sediments requires that the Mn is prevented from diffusing out of the

sediment when accumulation continues and the sediment becomes anoxic. As noted earlier, sulphate reduction can convert Mn oxyhydroxide phases to Mn carbonate phases, fixing them within the sediment. Possibly, then, the enhanced Mn content in the earliest Holocene sediments occurs as a diagenetic Mn carbonate or as a residual detrital phase; the latter would be resistant to redox processes.

4.1.2. The mid-Holocene sediment record (∼7000–4000 cal. years BP)

The PI core records a major change in geochemistry and in magnetic properties within the mid-Holocene. The interval 365–335 cm (∼7000–3800 cal. years BP) displays the highest average content of sulphur, iron, and mud for the core; the start of the interval is approximately coeval with age estimates for the emplacement of barriers along the NSW coast [61,55]. The core maximum sulphur value is achieved at 340 cm, coincident with the upper boundary of the dramatic drop in magnetic parameters (Fig. 5), a factor-of-two reduction in the Mn:Fe ratio (Fig. 10) and the loss of iron staining from the sand fraction. The decrease in the ferrimagnetic content and in the interparametric magnetic ratios resulted from the complete loss of magnetosomes. This loss occurs over the interval 350–340 cm, equivalent to a sediment age of ∼5000–4100 cal. years BP.

At the CB site, the Thom and Roy [63] sea-level curve suggests that inundation occurred between ∼8400 and 8100 cal. years BP; however, a radiocarbon date of 6000 (±450) cal. years BP, from a sample collected 2 cm above the Holocene–Pleistocene boundary, indicates that the onset of Holocene accumulation at the CB site was approximately coincident with termination of the transgression and ∼1500 years after inundation. Considerable reworking occurred at the site prior to the onset of sediment accumulation, reflecting the exposure of the core site to appreciable wave ravinement during the marine transgression. The mid-Holocene sediments at the CB site (244–229 cm) are notably coarser than the overlying sediments containing a mix of medium/fine sand and clay, poorly-preserved shell fragments and rare, pyritized specimens of *A. beccarii*; the sediment also accumulated extremely slowly, with only 13 cm of sediment between ∼6000 and 4000 cal. years BP. The sediment characteristics and slow rate of accumulation suggest that following the transgression, higher energy conditions continued at the site until some time shortly before the shell layer began to accumulate at ∼4000 cal. years BP. The delay in the onset of sediment accumulation, together with the character of the earliest sediment, indicates that the site was exposed to significant wave action and/or water currents for a considerable period following marine flooding. Without taking into account any potential reservoir effects in the carbon dating, this would explain the apparent shell lag in the 14-carbon age dates. Furthermore, in common with the PI core, the earliest Holocene sediment in the CB core contains both magnetosomes and pyrite; this co-occurrence, which continues in to the late Holocene sediments, is discussed below.

4.1.3. The late-Holocene sediment record (4000 cal. years BP – present)

At the PI site, the iron and sulphur contents are approximately halved between 340 and 320 cm, the slightly larger decrease in iron content leading to a drop in the Fe av:S ratio to values that fall between the Fe:S ratio of stoichiometric pyrite and that of iron monosulphide. We interpret the above behaviour as evidence that the system has become iron limited; above 340 cm, the majority of the reactive iron has been converted to pyrite and the total sulphide content decreases in response to the decline in available iron. The availability of reactive iron, labile organic material and dissolved sulphate are controlling factors in iron sulphide formation [4]. Most iron within silicate minerals will not be available

for reduction or pyritisation on the time scales pertinent to this study [51]. Iron limitation will result in an excess of dissolved sulphide in the sediment, which is consistent with the narrow peak in Cu that occurs within the interval 310–315 cm. The onset of iron-limited conditions coincides with a large decrease in mud content (particularly the silt component). These changes are consistent with a decline in fluvial influence at the PI site. The grain-size data indicate episodic influxes of marine sand, centred at depths of 320, 280 and 250 cm; following each of these sand pulses there is a brief recovery in the mud content, suggesting that the interval ∼330–230 cm (∼3600–1700 cal. years BP) sees the periodic migration of tidal channel sands in response to waxing and waning river flows or to episodes of enhanced tidal currents through the entrance channel. Subsequently, the interval 230–190 cm sees a gradual transition to the flood-tide delta of unit 1.

Towards the top of unit 2 in the PI core (∼1800 cal. years BP), and partly coincident with the zone of bioturbation, a distinct drop in ferrimagnetic content (SIRM, ARM) corresponds with the coupled decrease in iron and mud content. The loss of ferrimagnetic material is followed in the unit 2/unit 1 transition zone by a small increase in the ferrimagnetic content and by a significant decrease in ferrimagnetic grain size (increase in the interparametric ratios). We suggest that the production of magnetosomes in the lower part of unit 1 was facilitated by the migration of Fe^{2+} from the upper part of unit 2. This mechanism requires that bacterially mediated iron reduction, rather than sulphate reduction, is occurring in the top of unit 2; macrobenthic bioturbation has been shown to increase the rate and depth penetration of organic matter degradation and to inhibit sulphate reduction, thereby diminishing the abiotic reduction of iron by sulphide (pyritisation) in favour of the bacterial reduction of iron [24,33].

For most of unit 1 (∼1800-present cal. years BP), the mud content of the PI core remains uniformly low, reflecting the proximity of the entrance channel and the predominant supply of sand from the flood-tide delta. Mud content increases in the top of the core, consistent with human activity in the catchment; the extension of this muddy interval to a depth of −40 cm (∼300 cal. years BP) suggests that human activity of the last ∼150 years has produced a significant increase in sediment accumulation rate. The magnetic character of unit 1 alternates between intervals with a significant magnetosome content (200–150 cm; 120–50 cm) and the remaining intervals that show a lower ferrimagnetic content and coarser magnetic grain-size. The latter core intervals coincide with zones of increased sulphur content, indicating a transition to periods of sulphate reduction and the pyritisation of the available iron. The lower of these zones (150–120 cm) coincides with a brief interval of increased clay and organic matter content, while the upper zone, which corresponds with the muddy core-top, incorporates the modern redox boundary.

We also note that the upper 40 cm of unit 1 shows enhanced values of Al-normalised Mo content. The broad Mo/Al peak in the upper 20 cm may be associated with anthropogenic input or with the release of Mo during Mn reduction [6]; however, the large-amplitude Mo/Al peak at 40 m depth is associated with smaller-amplitude peaks in %TOC, %Fe and %S content. Scavenging of Mo by organic matter has been recognised in estuarine sediments, following which the scavenged Mo may become fixed as a sulphide phase within anoxic sediment [37]. We do not see a decrease in the abundance of agglutinated foraminifera at this depth, which implies that sulphide generation was limited by the low content of labile organic matter.

In the CB core, the sediment shows the continuation of an upward increasing trend that began at ∼235 cm, in both the absolute sulphur and iron content. The increase in S and Fe corresponds to a trend of increasing mud content; however, while the Al-normalised Fe remains constant, Al-normalised S increases to a local maximum between 220 and 210 cm, indicating significant S enhancement that is unrelated to mud content and must reflect increased sulphide formation. Within this interval (220–210 cm), Fe_{av}/S drops to a value close to that of stoichiometric iron monosulphide, confirming that most of the iron content has been converted to an iron sulphide. However, although the magnetic data indicates a small decrease in the ferrimagnetic content of this short interval (a local minimum in ARM and SIRM from 212–220 cm), the character of the ferrimagnetic material is unchanged, with the ARM/SIRM value remaining consistent with single domain magnetosomes (ARM/SIRM). Taken together, the data suggest that enhanced sulphide formation in the interval ∼220–210 cm has resulted in a reduction in the amount of reactive iron that remains available for the formation of magnetosomes, but that sufficient iron remains for the magnetosomes to dominate the ferrimagnetic content. This observation supports our contention that the formation of magnetosomes occurs after sulphide formation has terminated but while some reactive iron still remains within the sediment. As we argued for the PI core, the high iron content of the earliest muddy sediments will facilitate the exhaustion of sulphide before the reactive iron is consumed; also in common with the PI core, this interpretation is supported by the retention of an iron oxide coating on the sand fraction of the basal Holocene interval. However, the behaviour exhibited between 220 and 210 cm by F/Al, S/Al, Fe_{av}/S and the magnetic parameters indicates that an additional factor is important in determining the extent to which the reactive iron is consumed by sulphide.

The shell content of the interval may reveal the controlling factor in modern settings; the biological activity of shelled fauna has been shown to impact on redox conditions by triggering sulphate reduction [14]. In support of the influence of the shell layer, between 225 and 205 cm (∼2800 cal. years BP) the Mn:Fe ratio is halved, with the Mn:Fe minimum at 205 cm being accompanied by minima in the Al-normalised trace elements V, Cr and Zn (and to a lesser extent Ni, Cu and U). Sorption of trace elements to Fe–Mn oxyhydroxides occurs in marine environments [34] and these trace elements will be remobilised and may undergo diffusion during the subsequent dissolution of the Fe and Mn phases [5]. The iron content does not decrease at this level, which suggests that dissolved iron became trapped as pyrite or magnetosomes. The Al-normalised As content shows enhanced values below 205 cm, similar to the Al-normalised Fe values and suggesting that arsenic originally adsorbed to iron oxyhydroxides has been released during iron reduction and then become trapped in the sediment as an insoluble sulphide phase [31,44,43]. The subsequent interval of low sulphur content (∼205–185 cm), which extends some 12–17 cm above the shell layer, corresponds with a small decrease in the total iron content (which impacts strongly on the Fe/Al ratio) and with a Mo content that is below instrumental resolution. The interval also sees a modest increase in the sand content, which displays an iron coating, and as noted earlier, the interval also has visible wood and charcoal fragments. We also noted that the upper part of the shell layer shows an increasing proportion of fragments and that these fragments fine upwards, consistent with reworking of the top of the shell layer and conceivably the overlying sediments. Pyrite oxidation would accompany reworking, leading to the observed increase in the Fe_{av}/S ratio and the loss of sulphide-hosted trace elements (e.g. Mo, Ni, As).

Immediately above the reworked interval there is an abrupt increase in sulphur content that coincides with a decline in the ferrimagnetic content (between 182 and 178 cm) and with the loss of iron staining on the sand fraction. Although these changes do not coincide with a major change in the texture of the clastic material or in the total iron content, we note that the Fe/Al ratio above the reworked interval is distinctly lower than the ratio below the interval. This decline in the ratio indicates that there has either been a

transformation in the type of clay, with a more iron-rich clay found below the reworked zone, or there has been a change in the distribution of the iron, with a larger part of the iron content associated with the coarser fraction below the reworked zone. The behaviour seen above the reworked interval is consistent with the onset, at ~2600 cal. years BP, of conditions suited to the accumulation of central basin mud.

In the CB core, the transition to unit 1 sees a decrease in mud content that reflects the encroachment of the bay-head delta. In common with the PI core, mud content remains at low levels throughout most of unit 1. Unlike the PI core, ferrimagnetic content decreases through the transition zone and remains low throughout the unit; there is also an absence of magnetosomes and the sand content remains uniformly grey, indicating that the diagenetic removal of iron staining is persistent throughout the unit. The modern redox boundary occurs at ~10 cm depth, associated with an increase in mud content at the top of the core.

4.2. Proxy signals of palaeo-environmental change

The previous discussion clearly identifies the imprint of the rising sea levels associated with the post-glacial marine transgression. In the context of current concerns over sea level rise, it is important to consider the sensitivity with which Holocene estuaries have responded to smaller changes in sea level and regional climate. The CB and PI data allows us to evaluate the mid- to late-Holocene environmental response at two important sites within the Tuggerah Lake estuary. At high-stand, sea-level was up to 2 m higher than at present [71], with data from Northern NSW [22] suggesting that sea level was more than l m above present level until some time between 3200 and 1800 cal. years BP. An interpretation of fixed biological indicators from Port Hacking, ~100 km south of Tuggerah Lake [2], has provided a more detailed chronology of late Holocene sea level. The data suggest that: (a) sea level was ~1.5–1.7 m above present level from at least ~4150 radiocarbon years BP (~6000 cal. years BP), and perhaps as far back as ~5200 radiocarbon years BP (~4700 cal. years BP), by inference from sea level at magnetic Island; [35] to ~3500 radiocarbon years BP (3900 cal. years BP); (b) sea level fell by ~0.5 m between ~3500 and 2800 radiocarbon years BP (~3900–3000 cal. years BP); (c) between 2100 and 1800 radiocarbon years BP (2100–1700 cal. years BP) sea-level may have increased, and then fallen, by approximately 0.3 m; (d) sea level has fallen by 0.8 m between 1400 radiocarbon years BP (~1200 cal. years BP) and the present.

In terms of regional climate, pollen records from southeast Australia [36,39] indicate that effective precipitation reached a Holocene maximum between 7500 and 4600 cal. years BP, after which drier conditions have prevailed. A marine record from south Australia supports a switch from generally wetter conditions during the early Holocene to a subsequent decrease in temperature and aridity from ~6.5 ka [9]. The interval of maximum effective precipitation is supported by evidence for maximum lake levels in the region at ~6000 cal. years BP [28], while the subsequent onset of regional aridity is supported by evidence of declining flows in the Murray River (South Australia; [12]), between ~5800 and 4000 cal. years BP, at which point the river entrance became constricted. These regional climate indicators are consistent with evidence for a major change in the ENSO climate system; the onset of modern ENSO periodicities occurs at ~5000 years BP [25,10], and subsequently, ENSO amplitude increased abruptly at ~2700 cal. years BP, reaching a maximum between ~2300 and 1700 cal. years BP [13,70,25].

At the CB site, the characteristics of the mid-Holocene sediment (slow accumulation, relatively coarse-grained, and shell fragments) suggest an interval dominated by erosion/reworking, consistent with the continued exposure of the site to oceanic

currents and wave action prior to the emergence of the Holocene barrier system. Conversely, however, the PI site experienced quiet conditions during the early- to mid-Holocene, with slightly-sandy mud accumulating between ~8600 and 5000 cal. years BP, suggesting that the PI site was protected from the oceanic influence. The seismic and borehole data of Roy and Peat [53] delineate a series of low-stand fluvial channels that coalesce as a broad channel that exits the current lake some distance to the north of the present entrance channel. Low-stand excavation of the Pleistocene barrier at this location would have acted as the focus of the initial ingress of ocean water and marine sand during the transgression. The PI site lies to the south of this breach and the residual section of the Pleistocene barrier may have protected the PI site from the full effects of oceanic currents and waves.

However, there may be an alternative mechanism responsible for the high-energy conditions seen at the CB site. Entering the western margin of the lake, the higher river flows of the mid-Holocene (a consequence of the high levels of effective precipitation noted above) could have generated high energy conditions at the CB site, while having little influence at the PI site. At ~4000 cal. years BP, conditions at the CB site had changed sufficiently to allow colonisation by *Notospisula*, with sedimentation restricted to an impoverished supply of mud. This date seems too late for the change in conditions to have been brought about by a major growth in the barrier complex, but the transition may have resulted from barrier emergence, as a consequence of falling sea level. Our study site lies on the north-eastern corner of a larger zone of southeastern Australia that underwent major increases in climatic aridity and decline in river flows after ~5000 cal. years BP [12], which may have also contributed to the change in conditions at the CB site. The shell layer accumulated gradually over the next ~1000 years, some time after which the upper part of the layer was reworked. The proximity of the CB site to the source of freshwater input is reflected by the supply of finer-grained sediment. Within the remainder of unit 2, the CB core shows an increased content of wood and charcoal fragments, the sediment accumulation rate increases and *Notospisula* is restricted to thin layers that show an increasingly fragmentary nature as the bay-head delta sand of unit l is approached. These data suggest that conditions at the CB site were only intermittently suited to colonisation, perhaps as a result of the increasing influence of sediment delivered by Ourimbah Creek; falling sea level would contribute to the progradation of the bay-head delta, with the unit 2/unit 1 transition indicating that the delta front reached the CB site at ~1100 cal. years BP.

At the PI site, multi-proxy evidence (see geochemistry section) indicates a gradual increase in the proportion of marine sand after ~4900 cal. years BP, reaching a local maximum at ~3100 cal. years BP. It is possible that the increasing marine sand component is the result of reduced fluvial input, as the timing is consistent with regional evidence of declining river flows [12]. Alternatively, the declining fluvial input of sediment at the PI site may point instead to the growing influence of marine water at the site, due to the increasing proximity of the entrance channel. As noted above, seismic and borehole data [53] suggests that the entrance channel was initially located further north, whereas the current location of the entrance channel, at the southern limit of the barrier system, is bedrock controlled. Therefore, the PI core may record the southward migration of the tidal entrance, driven by the redistribution of barrier and beach sands by a combination of deflation and longshore drift. The fall in sea level between ~3900 and 3000 cal. years BP may also have had a contributory effect; falling sea level would have lead to incision and reworking of the flood-tide delta and shoaling of the entrance channel, perhaps leading to the re-establishment of tidal

exchange at the location of the present tidal channel. Encroachment of the relocated floodtide delta towards the PI site leads to the increasing delivery of sand, culminating in the arrival of the delta front between 1600 and 1400 cal. years BP. Evidence in support of barrier reworking is provided by radiocarbon dates obtained from the interval between 247 cm and the top of unit 2. The two dates that were obtained from wood/charcoal fragments (5175 ± 145 at 247 cm; 7505 ± 85 at 225 cm; both cal. years BP) are considerably older than predicted by the age model and show an age reversal, consistent with increasing incision of the barrier.

Following the initial increase in marine sand (see geochemistry section), that occurs between ~4900 and 3100 cal. years BP, the PI core shows the periodic recovery of the fluvial mud component between ~2800–2300, ~2200–2000 and ~1900–1700 cal. years BP, with the intervening periods showing a return to the predominance of marine sand. Instrumental records of precipitation and river flows from NSW indicate that the climate of the last century switched abruptly between flood- and drought-dominated intervals [21,19], a consequence of ENSO variability interacting with the Interdecadal Pacific Oscillation [48,23,32,68]. Therefore, it is reasonable to propose that the interval ~2700–1700 cal. years BP, which as noted above corresponds with the period of maximum late-Holocene ENSO variability [13,70] would have seen similar climate variability, with the potential for intervals of drought to alternate rapidly with periods of intense precipitation and enhanced river flows.

The first of the fluvial episodes, from ~2700 to 2400 cal. years BP in the PI core, corresponds with an interval of increased sand content at the CB site. This correlation is consistent with a period of increased fluvial energy, delivering an increased load of fluvial mud to the PI site and reversing the trend of increasing marine sand, while at the CB site reworking the top of the shell layer and producing a small shift to a coarser fluvial component. The two subsequent fluvial episodes, centred at ~2100 and 1700 cal. years BP, result in an increased mud content at both the PI and CB sites, most notably in the episode centred at ~2100 cal. years BP. At the CB site they appear by comparison to be muted events, because of the generally greater mud content of the CB core. An increase in hill-slope or riverbank erosion could increase the proportion of fines entering the lake, perhaps in response to a reduction in hill-slope cover and riparian vegetation. As noted by Prosser and Williams [50], although erosion rates in *Eucalyptus* forests around Sydney (~50 km from the study site) are typically very low (e.g. [49]), a combination of intense forest fires, followed by storms, can produce a 1000-fold increase in erosion. The enhanced ENSO variability of the period ~2500–1700 cal. years BP could produce an increase in drought-triggered fires, with erosion enhanced by the rapid alternation between periods of drought and intense precipitation. Wetland sediment records from Indonesia and Papua New Guinea [27] show a peak in regional fire frequencies between ~2300 and 1200 radiocarbon years BP, which the authors link to the interval of enhanced ENSO variability.

In addition to enhanced ENSO variability, changes in sea level would have contributed to the observed variation in fluvial sediment supply. The fall in sea level between ~3900 and 3000 cal. years BP would have increased the river gradient, leading to fluvial incision and the delivery of a greater sediment load, with a coarser grain size; this process would explain the reworking of the top of the shell layer, some time after ~3200 cal. years BP, which immediately precedes the small increase in sand at the CB site and the major increase in mud at the PI site. In terms of the following fluvial episode, which increases the delivery of mud to both core sites, the proposed small increase in sea level between ~2100 and 1700 cal. years BP provides a potential mechanism. Increasing sea-level would cause a landward migration of fluvial delivery and a seaward retreat of flood tidal processes; these outcomes would lead to a coeval increase in mud content at both sites.

5. Conclusions

In this study we have presented multiple data sets obtained from two sediment cores, which provide a detailed history of the Holocene evolution of the Tuggerah Lake barrier estuary. Recognising that traditional lithostratigraphic studies of estuarine sediments have provided considerable insight into the physical evolution of estuaries, both on individual and conceptual levels, here we show that detailed, multidisciplinary investigations have the potential to extract information that pertains to subtle details of this physical evolution and, of equal importance, provides a link between the sedimentary record and the causative environmental processes that influence estuary evolution.

In terms of a first-order interpretation, the major lithological changes recognised at the Pelican Island and Chittaway Bay core sites reflect firstly the transgressive erosion of the early Holocene soil profile, followed by central basin estuarine deposition and secondly, the more recent transitions from a central basin setting to flood tide (PI) and bay head (CB) delta environments. These major changes are recognised through variations in the texture, geochemistry and magnetic properties of the sediments, and in the abundance and preservation of shelled fauna.

We have also identified a sequence of more subtle changes in the late Holocene sediment record that can be attributed to the onset of modern ENSO periodicities and a strengthening of the ENSO signal [25,10], perhaps in concert with small sea-level fluctuations [2], and a stronger East Australian current and warmer temperatures [29]. These environmental factors produced periodic changes in the delivery of fluvial mud to the lake and impacted on the exchange of water through the entrance channel. As a consequence, the Lake experienced an increase in mud content and faster sediment accumulation rates. The burial rate peaked between ~2500 and 1700 cal. years BP, an interval that includes the late-Holocene maximum in ENSO variability [13,70] and perhaps a ~0.3 m increase in sea level [2].

In terms of the acid sulphate potential of the sediments, as expected, the pyrite content of the sediments is sensitive to the availability of reactive iron. Increases in the oxidation of the labile organic component (slow accumulation rates and/or increased sediment permeability) produce conditions in which bacterial iron reduction increases at the expense of the abiotic pathway (pyritisation), Therefore, the pyrite content of the sediments is linked to the environmental factors discussed above. Moreover, while reworking of the antecedent land surface by the marine transgression has produced basal Holocene sediment that is richer in iron than at any time since, resulting in the incomplete pyritisation of the iron content during early infilling of the Lake. Under these circumstances, the production of biogenic (bacterial) magnetite has produced a magnetic signature that reveals the change in iron reduction pathway and the incomplete pyritisation of the iron content.

The stratigraphies revealed by the CB and PI cores are consistent with the earlier study of Roy and Peat [53], which showed that only minor fluvial incision occurred during the last sea level low stand (see Fig. 1). Such limited low-stand erosion is unusual for NSW estuaries (Lake Macquarie, a barrier estuary immediately north of the Tuggerah Lake system – approximately 90 km north of Sydney), experienced up to 27 m of low-stand incision; [52] and requires further investigation.

Acknowledgements

References

[1] Aitchison J. The statistical analysis of compositional data. New York: Chapman & Hall; 1986.

[2] Baker RGV, Haworth RJ. Smooth or oscillating late Holocene sea-level curve? Evidence from cross-regional statistical regressions of fixed biological indicators. Mar Geol 2000;163(1–4):353–65.

[3] Berner RA. Migration of iron and sulfur within anaerobic sediments during early diagenesis. Am J Sci 1969;267(1). 19-&.

[4] Berner RA. Sedimentary pyrite formation: an update. Geochim Cosmochim Acta 1984;48(4):605–15.

[5] Burdige DJ. The biogeochemistry of manganese and iron reduction in marine sediments. Earth Sci Rev 1993;35(3):249–84.

[6] Calvert SE, Pedersen TF. Geochemistry of recent oxic and anoxic marine sediments: implications for the geological record. Mar Geol 1993;113(1–2):67–88.

[7] Calvert SE, Pedersen TF. Sedimentary geochemistry of manganese: implications for the environment of formation of manganiferous black shales. Econ Geol Bull Soc Econ Geol 1996;91(1):36–47.

[8] Calvert SE, Price NB. Composition of manganese nodules and manganese carbonates from Loch Fyne, Scotland. Contrib Mineral Petrol 1970;29(3):251.

[9] Calvo E, Pelejero C, De Deckker P, Logan GA. Antarctic deglacial pattern in a 30 kyr record of sea surface temperature offshore South Australia. Geophys Res Lett 2007;34(13).

[10] Cane MA. The evolution of El Nino, past and future. Earth Planet Sci Lett 2005;230(3–4):227–40.

[11] Canfield DE. Reactive iron in marine sediments. Geochim Cosmochim Acta 1989;53(3):619–32.

[12] Cann JH, Bourman RP, Barnett EJ. Holocene foraminifera as indicators of relative estuarine-lagoonal and oceanic influences in estuarine sediments of the River Murray, South Australia. Quat Res 2000;53(3):378–91.

[13] Clement AC, Seager R, Cane MA. Suppression of El Nino during the mid-Holocene by changes in the Earth's orbit. Paleoceanography 2000;15(6):731–7.

[14] Dahlback B, Gunnarsson LAH. Sedimentation and sulfate reduction under a mussel culture. Mar Biol 1981;63(3):269–75.

[15] Daviescolley RJ, Nelson PO, Williamson KJ. Copper and cadmium uptake by estuarine sedimentary phases. Environ Sci Technol 1984;18(7):491–9.

[16] de Boer CB, Dekkers MJ. Grain-size dependence of the rock magnetic properties for a natural maghemite. Geophys Res Lett 1996;23(20):2815–8.

[17] Degroot AJ, Zschuppe KH, Salomons W. Standardization of methods of analysis for heavy-metals in sediments. Hydrobiologia 1982;91–92:689–95.

[18] Dellwig O, Watermann F, Brumsack HJ, Gerdes G. High-resolution reconstruction of a holocene coastal sequence (NW Germany) using inorganic geochemical data and diatom inventories. Estuar Coast Shelf Sci 1999;48(6):617–33.

[19] Erskine JM, Warner RF. Further assessment of flood- and drought-dominated regimes in south-eastern Australia. Aust Geogr 1998;29:257–61.

[20] Erskine WD. Flood-tidal and fluvial deltas of Tuggerah Lakes, Australia: human impacts on geomorphology, sedimentology, hydrodynamics and seagrasses. In: Young G, Perillo GM, editors. Deltas: landforms, ecosystems and human activities. IAHS Publication; 2013. p. 159–67.

[21] Erskine WD, Bell FC. Rainfall, floods and river channel changes in the upper Hunter. Aust Geogr Stud 1982;20:183–96.

[22] Flood PG, Frankel E. Late Holocene higher sea level indicators from eastern Australia. Mar Geol 1989;90(3):193–5.

[23] Franks SW, Kuczera G. Flood frequency analysis: evidence and implications of secular climate variability, New South Wales. Water Resour Res 2002;38(5).

[24] Furukawa Y, Smith AC, Kostka JE, Watkins J, Alexander CR. Quantification of macrobenthic effects on diagenesis using a multicomponent inverse model in salt marsh sediments. Limnol Oceanogr 2004;49(6):2058–72.

[25] Gagan MK, Hendy EJ, Haberle SG, Hantoro WS. Post-glacial evolution of the Indo-Pacific Warm Pool and El Nino-Southern Oscillation. Quatern Int 2004;118:127–43.

[26] Govindaraju K. Compilation of working values and sample description for 383 geostandards. Geostand Newsl 1994;18(2):1–158.

[27] Haberle SG, Hope GS, van der Kaars S. Biomass burning in Indonesia and Papua New Guinea: natural and human induced fire events in the fossil record. Palaeogeogr Palaeoclimatol Palaeoecol 2001;171(3–4):259–68.

[28] Harrison SP, Dodson J. Climates of Australia and New Guinea since 18,000 yr B.P. In: Global climates since the last glacial maximum; 1993.

[29] Harwoth RJ, Baker RGV, Flood PJ. A 6000 year-old Fossil Dugong from botany bay: inferences about changes in Sydney's climate, sea levels and waterways. Aust Geogr Soc 2004;42(1):46–59.

[30] Higginson FR. The distribution of submerged aquatic angiosperms in the Tuggerah Takes system. Proc Linn Soc New S Wales 1965;90(3):328–34.

[31] Huertadiaz MA, Morse JW. Pyritization of trace metals in anoxic marine sediments. Geochim Cosmochim Acta 1992;56(7):2681–702.

[32] Kiem AS, Franks SW, Kuczera G. Multi-decadal variability of flood risk. Geophys Res Lett 2003;30(2).

[33] Koretsky CM, Van Cappellen P, DiChristina TJ, Kostka JE, Lowe KL, Moore CM, et al. Salt marsh pore water geochemistry does not correlate with microbial community structure. Estuar Coast Shelf Sci 2005;62(1–2):233–51.

[34] Koschinsky A, Hein JR. Uptake of elements from seawater by ferromanganese crusts: solid-phase associations and seawater speciation. Mar Geol 2003;198(3–4):331–51.

[35] Larcombe P, Carter RM. Holocene bay sedimentation and sea-levels. Magnetic Island: Geological Society of Australia, Sydney; 1998.

[36] Lloyd PJ, Kershaw AP. Late quaternary vegetation and early Holocene quantitative climate estimates from Morwell Swamp, Latrobe Valley, south-eastern Australia. Aust J Bot 1997;45(3):549–63.

[37] Malcolm SJ. Early diagenesis of molybdenum in estuarine sediments. Mar Chem 1985;16(3):213–25.

[38] Mann S, Sparks NHC, Frankel RB, Bazylinski DA, Jannasch HW. Biomineralization of ferrimagnetic greigite (Fe3S4) and pyrite (FeS2) in a magnetotactive bacterium. Nature 1990;343(6255):258–61.

[39] McKenzie GM, Kershaw AP. A vegetation history and quantitative estimate of Holocene climate from Chapple Vale, in the Otway region of Victoria, Australia. Aust J Bot 1997;45(3):565–81.

[40] McNeil DH. Diagenetic regimes and the foraminiferal record in the Beaufort-Mackenzie basin and adjacent Cratonic areas. Ann Soc Geol Pol 1997;67:271–86.

[41] Morse JW, Luther GW. Chemical influences on trace metal-sulfide interactions in anoxic sediments. Geochim Cosmochim Acta 1999;63(19–20):3373–15.

[42] Moskowitz BM, Frankel RB, Bazylinski DA. Rock magnetic criteria for the detection of biogenic magnetite. Earth Planet Sci Lett 1993;120:283–300.

[43] Mucci A, Boudreau B, Guignard C. Diagenetic mobility of trace elements in sediments covered by a flash flood deposit: Mn, Fe and As. Appl Geochem 2003;18(7):1011–26.

[44] Mucci A, Richard LF, Lucotte M, Guignard C. The differential geochemical behavior of arsenic and phosphorus in the water column and sediments of the Saguenay Fjord estuary, Canada. Aquat Geochem 2000;6(3):293–324.

[45] Myers CR, Nealson KH. Bacterial manganese reduction and growth with manganese oxide as the sole electron acceptor. Science 1988;240(4857):1319–21.

[46] Postma D. Kinetics of nitrate reduction by detrital Fe(II) silicates. Geochim Cosmochim Acta 1990;54(3):903–8.

[47] Poulton SW, Krom MD, Raiswell R. A revised scheme for the reactivity of iron (oxyhydr)oxide minerals towards dissolved sulfide. Geochim Cosmochim Acta 2004;68(18):3703–15.

[48] Power S, Casey T, Folland C, Colman A, Mehta V. Inter-decadal modulation of the impact of ENSO on Australia. Clim Dyn 1999;15(5):319–24.

[49] Prosser IP, Chappell J, Gillespie R. Holocene valley aggradation and gully erosion in headwater catchments, south-eastern highland of Australia. Earth Surf Proc Land 1994;19(5):465–80.

[50] Prosser IP, Williams L. The effect of wildfire on runoff and erosion in native Eucalyptus forest. Hydrol Process 1998;12(2):251–65.

[51] Raiswell R, Canfield DE. Rates of reaction between silicate iron and dissolved sulfide in Peru Margin sediments. Geochim Cosmochim Acta 1996;60(15):2777–87.

[52] Roy PS. Holocene estuary evolution-stratigraphic studies from southeastern Australia. In: Dalrymple RW, Boyd R, Zaitlin BA, editors. Incised-valley systems: origin and sedimentary sequences. Society for Sedimentary Petrology; 1994. p. 241–64.

[53] Roy PS, Peat C. Bathymetry and bottom sediments of Lake Macquarie; 1973.

[54] Roy PS, Thom BG. Late Quaternary marine deposition in New South Wales and South Queensland – an evolutionary model. J Geol Soc Aust 1981;28(3–4):471–89.

[55] Roy PS, Thom BG, Wright LD. Holocene sequences on an embayed high-energy coast: an evolutionary mode. Sed Geol 1980;26(1–3):1–19.

[56] Schwertmann U, Taylor RM. Iron oxides. In: Minerals in soil environments. SSSA Book Series, No. 1; 1989. p. 379–438.

[57] Scott A. Ecological history of the Tuggerah Lakes final report, produced by CSIRO land and water and saintly and associates for Wyong Shire Council, Canberra; 1999.

[58] Shaw TJ, Gieskes JM, Jahnke RA. Early diagenesis in differing depositional environments: the response of transition metals in pore water. Geochim Cosmochim Acta 1990;54(5):1233–46.

[59] Skilbeck CG, Rolph TC, Hill N, Woods J, Wilkens RH. Holocene millennial/centennial-scale multiproxy cyclicity in temperate eastern Australian estuary sediments. J Quat Sci 2005;20(4):327–47.

[60] Suess E. Mineral phases in anoxic sediments by microbial decomposition of organic matter. Geochim Cosmochim Acta 1979;43(3):339.

[61] Thom BG, Polach H, Bowman GM. Holocene age structure of coastal sand barriers in N.S.W., Australia; 1978.

[62] Thom BG, Roy PS. Australian sea levels in the last 15,000 years: a review. James Cook University, Department of Geography; 1983.

[63] Thom BG, Roy PS. Relative sea levels and coastal sedimentation in southeast Australia in the Holocene. J Sediment Petrol 1985;55(2):257–64.

[64] Thomson J, Higgs NC, Colley S. Diagenetic redistributions of redox-sensitive elements in northeast Atlantic glacial/interglacial transition sediments. Earth Planet Sci Lett 1996;139(3–4):365–77.

[65] Torii M, Fukuma K, Horng CS, Lee TQ. Magnetic discrimination of pyrrhotite- and greigite-bearing sediment samples. Geophys Res Lett 1996;23(14):1813–6.

[66] Tudryn A, Tucholka P. Magnetic monitoring of thermal alteration for natural pyrite and greigite. Acta Geophys Pol 2004;52:509–20.

[67] Turekian KK, Wedepohl KH. Distribution of the elements in some major units of the earth's crust. Geol Soc Am Bull 1961;72(2):175–91.

[68] Verdon DC, Wyatt AM, Kiem AS, Franks SW. Multidecadal variability of rainfall and streamflow: Eastern Australia. Water Resour Res 2004;40(10).

[69] Wedepohl KH. Zinc and lead in common sedimentary rocks. Econ Geol 1971;66(2):240.

[70] Woodroffe CD, Beech MR, Gagan MK. Mid-late Holocene El Nino variability in the equatorial Pacific from coral microatolls. Geophys Res Lett 2003;30(7).

[71] Young RW, Bryant EA, Price DM. Last interglacial sea levels on the south coast of New South Wales. Aust Geogr 1993;24(2):72–5.